BILINGUAL PUBLISHING CO.
Pioneer of Global Academics Since 1984

02

Journal of Building Material Science

Volume 2 Issue 2 · December 2020 · ISSN: 2630-5216 (Online)

Volume 2 Issue 2 • December 2020 • ISSN 2630-5216 (Online)

JOURNAL OF BUILDING MATERIAL SCIENCE

BILINGUAL PUBLISHING CO.
Pioneer of Global Academics Since 1984

BILINGUAL PUBLISHING CO.
Pioneer of Global Academics Since 1984

Volume 2 | Issue 2 | December 2020 | Page 1-31
Journal of Building Material Science

Contents

Article

Review

BILINGUAL PUBLISHING CO.
Pioneer of Global Academics Since 1984

Journal of Building Material Science
https://ojs.bilpublishing.com/index.php/jbms

ARTICLE

Assessing the Ageing Impact on Fatigue-Life of Asphalt Concrete

Saad Issa Sarsam*

Sarsam and Associates Consult Bureau SACB. Baghdad, Iraq

ARTICLE INFO

Article history
Received: 11 January 2021
Accepted: 2 March 2021
Published Online: 30 March 2021

Keywords:
Fatigue life
Asphalt concrete
Flexure strain
Ageing
Temperature
Strain level

ABSTRACT

The fatigue-life of asphalt concrete is often related to environmental condition, loading condition, ageing, material composition and properties. This work investigates the influence of short and long term ageing of laboratory beam specimens, asphalt percent, and testing temperature on fatigue life of asphalt concrete wearing course. Slab samples of (30 x 40 x 6) cm have been prepared, beam specimens of (40 x 5 x 6) cm were extracted from the asphalt concrete slab samples and tested for fatigue-life under the impact of three levels of micro strain (250, 400, and [3] 750) at (5, 20, and 30) °C before and after practicing long-term aging. It was observed that the fatigue-life decreased by (85 and 97) %, (87.5 and 97.4) %, (71.4 and 95.2) % after increasing the applied microstrain from (250 to 400 and 750) με for control mixture and for mixtures subjected to short- and long-term ageing processes respectively. The fatigue-life increased by (142.8 and 257.1) %, (34.4 and 57.8) % and (10 and 30) % when the asphalt content increased from (4.4 to 4.9 and 5.4) % for specimens practicing the applied microstrain of (250, 400 and 750) με respectively. It can be concluded that the fatigue life increases by a range of (two to fifteen) folds when the testing temperature increases from (5 to 20 and 30)°C respectively.

1. Introduction

One of the important parameters for the structural design of asphalt concrete pavements is the assessment of fatigue-life of the asphalt concrete mixture, which can be determined by implementing cyclic-fatigue tests in the laboratory. Golchin and Mansourian [1] evaluated fatigue properties and fatigue-life of asphalt concrete mixtures by implementing the four-point bending-beam test. Analysis of the tests results showed that the mixtures tested at lower strain levels, had higher final stiffness while the-fatigue life of specimens increased when the level of testing strains decreased. Song-tao et al. [2] stated that the problems of asphalt aging have not been comprehensively considered when pavement is designed globally, so the effects of aging on the life of asphalt pavement have not been studied accurately. The study of fatigue performance in different degrees of aging plays a significant role in improving design parameters and asphalt mixtures, and preventing early damage, as well as improving road performance and extending the life of asphalt pavement. Aging process of asphalt binder occurs in three stages: the first stage occures very fast during the production process of asphalt mixtures. Such stage is referred to as short-term aging process. The second stage of binder aging occurs at a slower rate during the transportation of the mixtures to the laying site, laying down and compaction of the mixture. The third stage occurs after construction while the asphalt concrete is in service

**Corresponding Author:*
Saad Issa Sarsam,
Sarsam and Associates Consult Bureau SACB. Baghdad, Iraq;
Email: saadisasarsam@coeng.uobaghdad.edu.iq

 DOI: https://doi.org/10.30564/jbms.v2i2.2792

and exposed to the surrounding environment as reported by Glover et al. [3]. Paul et al. [4] stated that aging of asphalt concrete continues for two to three years until the mixture approaches to its maximum density, and no further densification may occur. Aging can affect the physical properties of asphalt concrete mixture significantly, and hence affecting the performance of the asphalt pavement. However, it is required to characterize the aged asphalt mixture properly for achieving the successful design of asphalt pavements. A study by Al-Khateeb and Alqudahaims [5] investigated the impact of laboratory aging on the fatigue-life performance of asphalt mixtures. The mixtures were subjected to short and long term ageing then tested for fatigue using indirect tensile and various initial strain levels. It was found that the short term ageing led to an increase in fatigue-life. Findings also showed that the fatigue-life increased as the testing temperature increase. The evolution of permanent strain, fatigue-life, and resilient modulus of an asphaltic concrete mixture exposed under weather conditions was investigated by Quintana and Lizcano [6]. It was concluded that resilient modulus of the asphalt mixtures increases by more than two folds during 48 months of continuous exposure under the test environmental conditions. Such stiffness increase exhibits an increment of approximately ten folds in the mixture fatigue-life because of the binder stiffening effect due to its own ageing condition.The effect of ageing and temperature on the fatigue-life of asphalt concrete specimens made with two binder types, was studied by López-Montero and Miró [7]. Specimens have practiced an accelerated laboratory-ageing process, then were tested by using the strain sweep test at different testing temperatures of (-5, 5 and 20) °C. Test results were compared with those obtained from the un-aged specimens, it is showing the relative importance of ageing and temperature on the parameters which determine the fatigue-life of the asphalt mixture. The asphalt concrete mixtures behaviour becomes more brittle after practicing ageing process and the reduction of testing temperature. However, ageing process can hardly has an effect on fatigue-life at lower temperatures. As reported by Sol-Sánchez et al. [8], bituminous mixtures are designed and manufactured to withstand the traffic loads imposed, and also to resist the action of the environment. It was reported that it is necessary to carefully investigate all the variables that influence ageing. In fact, the ageing of asphalt concrete mixtures depends on multiple factors, such as air temperature, and availability of rain water, which therefore can have a great influence on the durability of asphalt mixtures. Sarsam [9] studied the impact of ageing on the stiffness of asphalt concrete beam specimens through the fatigue process. It was concluded that the stiffness is susceptible to moisture damage and aging, the increase in Microstrain level leads to a remarkable reduction in initial and failure stiffness's. The stiffness is susceptible to the testing temperature and asphalt content, lower testing temperature of 5º C exhibits higher stiffness value, while higher binder content has a negative impact on the stiffness. The effect of aging process on the fatigue properties of polymer-modified asphalt mixtures were assessed by Zhu et al. [10]. Two kinds of aging techniques were adopted, the first one is the short-time aging, while the second one is the natural-aging of the original specimen as exposed in the sunlight, and subjected to the rain and temperature changes for three, six, and nine months. Four-Point Bending beam test was conducted on the specimens to evaluate the fatigue-life properties of aged-asphalt mixtures at 15°C and the test results were compared with the original specimens. Test results indicated that the fatigue-life of aged-specimen decreases significantly when it was compared with the original ones, especially of the natural-aged specimens. Miró et al. [11] examined the combined influence of the loss of volatiles from the binder and the oxidation produced during the ageing process on the fatigue behaviour of the bitumen. Different temperatures have been implemented for evaluating the effect of visco-elastic phenomena on aged binder fatigue. The test results showed that the testing-temperature plays an important role in the influence of ageing on the fatigue response of bituminous binders, and in the mechanical response of these materials. Sarsam and AL-Lamy [12] stated that fatigue-life is the process of cumulative damage of asphalt pavement and it is one of the major causes of cracking. The traditional fatigue-life approach states that damage may occur in asphalt concrete specimen after practicing dynamic-repetitive loading which leads to fatigue-failure of the specimen. The number of load repetitions to failure equal to the fatigue-life, and can be calculated based on stress, or strain. The results of repeated four-point flexural-fatigue beam testing conducted by Sarsam and Alwan [13] have indicated that fatigue-life decreased by 70 percent after subjecting the asphalt concrete specimens to moisture damage process. For a Microstrain range from (250 to 400), the fatigue-life decreased by 87 percent as compared to reference mixture. Karakas [14] stated that exposure of asphalt pavement to environmental-conditions such as traffic and climate is one of the prominent ageing reasons for asphalt binder. The common mechanism of binder aging is the chemical-degradation in the structure of the binder by oxidation. Aging of asphalt binder can cause several serious distress issues of the asphalt pavement such as stiffening and stripping which may accelerates the formation of fatigue-cracking, and moisture-induced damage problems such as raveling, and potholes. The aim of the present investigation is to assess the impact of short and long term

DOI: https://doi.org/10.30564/jbms.v2i2.2792

ageing process, testing temperature, asphalt content, and strain levels on the fatigue-life of asphalt concrete wearing course by implementing the repeated four-point flexure test.

2. Materials Properties and Testing Methods

The materials implemented in the present assessment are economicaly available, and usually used by roadway agencies for asphalt pavement construction in Iraq.

2.1 Asphalt Cement

Asphalt binder with penetration graded of (40-50) was utilized in this assessment. It is obtained from AL-Naesria oil Refinery. The properties of asphalt cement comply with the SCRB [15] requirements. The physical properties of the asphalt binder are presented in Table 1.

Table 1. Physical Properties of Asphalt Binder

Property	Test Conditions	ASTM [16] Designation	Value	SCRB [15]
Penetration (0.1 mm)	25 °C , 100 gm, 5 seconds	D5-06	42	40-50
Softening Point (°C)	(Ring and Ball)	D36-895	49	-
Ductility (Cm)	25 ° C, 5 Cm/minutes	D113-99	136	>100
Specific Gravity	25 °C	D70	1.04	-
Flash Point (°C)	Cleaveland open cup	D92-05	256	>232
Properties After Thin Film Oven Test as per D1754-97				
Penetration (0.1mm)	25 °C , 100 gm, 5 seconds	D5-06	33	< 55 %
Ductility (Cm)	25 °C, 5Cm/minutes	D113-99	83	>25 %

2.2 Fine and Coarse Aggregates

Crushed coarse aggregates (passing sieve size 19 mm and retained on sieve No. 4) was brought from AL-Ukhaider quarry. A mixture of natural and crushed sand was implemented as fine aggregates (particle passing sieve No. 4 and retained on sieve No.200) as per SCRB [15] specification. The sand was brought from the same source. The physical properties of fine and coarse aggregates are demonstrated in Table 2.

Table 2. Physical Properties of Fine and Coarse Aggregates

Property	Coarse aggregates	ASTM [16] Designation	Fine aggregates	ASTM [16] Designation
Bulk Specific Gravity	2.542	C127-01	2.558	C128-01
Percent Water Absorption	1.07%	C127-01	1.83%	C128-01
Percent Wear (Los Angeles abrasion Test)	18%	C131-03	-------	--------

2.3. Mineral Filler

The mineral filler implemented in the present work is the limestone dust, it is mostly passing sieve No.200. It was brought from Karbala governorate. The physical properties of the mineral filler are exhibited in Table 3.

Table 3. Physical Properties of the Mineral Filler

Property	Bulk Specific Gravity	Percent Passing Sieve No. 200
	2.617	94

2.4 Selection of Aggregates Gradation

The selected aggregates gradation in this assessment follows the wearing course requirement as per SCRB [15] specification. It has a nominal maximum size of (12.5 mm). Table 4 shows the implemented aggregates gradation.

Table 4. Implemented Gradation for Combined Aggregates

Sieve size (mm)	Passing by weight%	
	Selected Gradation	SCRB [15] Specification
19	100	100
12.5	95	90-100
9.5	83	76-90
4.75	59	44-74
2.36	43	25-58
0.3	13	5-21
0.075	7	4-10

2.5 Preparation of the Asphalt Concrete Mixture

Aggregates were subjected to oven drying to a constant weight at 110ºC, and then sieved to different sizes and each size was separately stored. Fine and coarse aggregates were recombined with the specific percentage of mineral filler to meet the SCRB [15] specifications. The combined aggregates were then heated to 160º C, while the asphalt binder was separately heated to a temperature of 150º C. The desired amount of Asphalt binder was added to the heated aggregates and mixed thoroughly using a mechanical mixer for three minutes until all aggregate particles were coated with a thin film of asphalt binder. The asphalt concrete mixture was subjected to short-term oven aging for four hours at a temperature of 135 ºC as per AASHTO [17]. Asphalt concrete mixtures were prepared at optimum asphalt content of 4.9% and

DOI: https://doi.org/10.30564/jbms.v2i2.2792

at asphalt contents of 0.5 percent below and above the optimum, (4.4 and 5.4) %. The process of finding the optimum asphalt content was based on Marshall Properties as per AASHTO [17], the details could be found at Sarsam and Alwan [13]. Slab samples of (400 x 300 x 60) mm were prepared using the rolling compaction technique to the target bulk density according to EN12697-33 [18]. Beam specimens of (5 x 6 x 40) cm sizes were extruded from the slab using the diamond saw. Beam specimens were conditioned to long-term aging as per AASHTO [19] procedure. Figure 1 exhibits the long-term ageing process.

2.6. Determination of Fatigue Life with the Aid of Repeated Flexural Beam-Fatigue Test

The repeated-flexural beam fatigue test was implemented on the beam specimens as per AASHTO T 321 [20]. Asphalt concrete beams were placed in the four-point loading apparatus. Three testing temperatures of (30, 20, and 5) °C have been implemented. On the other hand, three different Microstrain levels of 250, 400, and 750 were tried to simulate various modes of loading in the field. The flexural-fatigue test is performed by placing the asphalt concrete beam specimen in the repetitive four-points loading chamber and application of specified strain level and testing temperature. Throughout the test, the beam was held in place by four clamps and the repeated sinusoidal load was applied to the two inner clamps with the outer clamps providing a reaction load. Such setup provides a constant bending moment over the central portion of the beam between the two inside clamps. The number of load cycles to failure was then recorded which gave an estimation of a particular mixture's fatigue-life. Figure 2 exhibits the four-point bending beam test setup.

Figure 1. Long-term ageing process

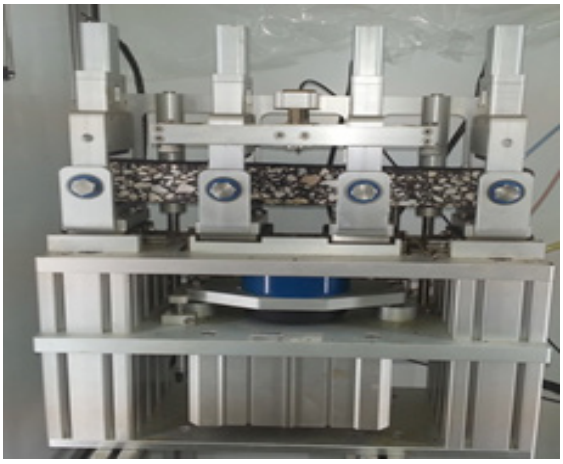

Figure 2. Four-point bending beam test setup

3. Discussions on Test Results

3.1 Evaluation of Fatigue-Life

Fatigue-life measurements were conducted at microstrain levels of 750, 400, and 250, a frequency level of 5Hz, testing temperature of (5, 20, and 30) °C, and three percentages of asphalt contents. Log-log Plots were established between the fatigue life (Nf) and the above-mentioned variables. The most important parameters for fatigue life assessment are the intercept, and the slope of the fatigue-life curve. The prepared asphalt concrete mixture was separated to three lots. The first lot was denoted as the control mixtures. The control mixture was compacted in the roller compactor and a slab sample was obtained. Beam specimens were extracted from the slabs and tested for fatigue life. The second lot had practiced the short-term ageing as per AASHTO [19] procedure, then it was compacted to slab samples. Beam specimens were extracted from the slabs of the second lot and tested for fatigue life. The third lot was subjected to short term ageing, and then it was compacted to slab samples. Beam specimens were extracted from the slabs of the third lot and subjected to long-term ageing as per AASHTO [20], then tested for fatigue life.

3.2 Influence of Ageing on Fatigue-Life for Asphalt Concrete

The fatigue life of asphalt concrete was evaluated by implementing the repeated-flexural beam-fatigue test on the beam specimens as per AASHTO T 321 [20]. Figure 3 demonstrate the influence of ageing process on the fatigue-life. It can be observed that the fatigue-life decreases for asphalt concrete after practicing the ageing process regardless of the ageing technique implemented.

DOI: https://doi.org/10.30564/jbms.v2i2.2792

When the applied microstrain level was low (250 με), the fatigue-life decreases by (16.4 and 77.5) % after practicing short- and long-term ageing respectively. When the applied microstrain level was moderate (400 με), the fatigue-life decreases by (30.3 and 57) % after practicing short- and long-term ageing respectively. However, after application of high level of microstrain (750 με), the reduction in fatigue-life was (31.4 and 65.5) % after practicing short- and long-term ageing respectively.

However, the fatigue-life decreases by (85 and 97) %, (87.5 and 97.4) %, (71.4 and 95.2) % after increasing the applied microstrain from (250 to 400 and 750) με for control mixture and for mixtures subjected to short-and long-term ageing processes respectively. Similar findings are addressed by Zhu et al. [10].

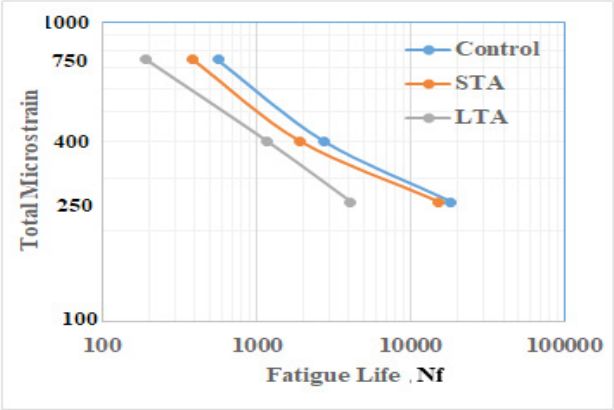

Figure 3. Influence of ageing process on the fatigue-life

Table 5 exhibits the fatigue-life parameters of asphalt concrete, the ageing process was able to decrease both intercepts which represent the total microstrain after the first load repetition (N =1), and the slope which represent the rate of deformation throughout the fatigue-life. Such observation indicates the stiffening of asphalt concrete after the ageing process. The power models relating the microstrain (με) with the fatigue-life (Nf) exhibit a strong coefficient of determination (R^2). Similar findings were reported by Sarsam and Alwan [21].

Table 5. Fatigue Parameters and Models for Asphalt Concrete Under Ageing

AC%	State	Fatigue Parameter		Models	Coefficient of Determination R^2
		Slope	Intercept		
4.9 %	Control mix	0.314	5214.3	$\mu\varepsilon = 5214.3\ Nf^{-0.314}$	0.981
	Short term Ageing	0.295	4113	$\mu\varepsilon = 4113\ Nf^{-0.295}$	0.974
	Long term Ageing	0.360	5015.3	$\mu\varepsilon = 5015.3\ Nf^{-0.36}$	0.998

3.3 Influence of Asphalt Binder on Fatigue-Life for Asphalt Concrete

Figure 4 depicts the influence of asphalt cement content on fatigue-life of asphalt concrete. It can be observed that the fatigue-life increases significantly as the binder content increases regardless of the applied microstrain. This could be attributed to the increase in asphalt cement film thickness which can possess a more durable mixture. It can be detected that at low microstrain level of (250 με), the fatigue-life increased by (142.8, 257.1) % when the asphalt binder content increased from (4.4 to 4.9 and 5.4) %. When the applied microstrain level was moderate (400 με), the fatigue-life increased by (34.4 and 57.8) % when the asphalt binder content increased from (4.4 to 4.9 and 5.4) %. However, after application of high level of microstrain (750 με), the improvement in fatigue-life was minimal in a range of (10-30) % as the asphalt content increases.

Table 6 exhibits the fatigue parameters of asphalt concrete at various asphalt percentages, increment of asphalt content was able to decrease both intercept and the slope, thus improving the flexibility of asphalt concrete. The power models relating the microstrain (με) with the fatigue life (Nf) at various binder content exhibit a strong coefficient of determination (R^2). Similar findings have been reported by Sarsam and AL- Lamy [22].

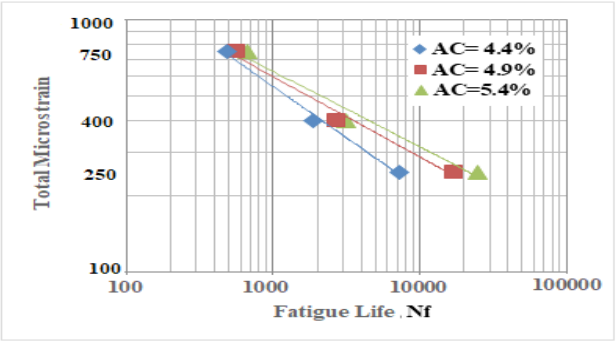

Figure 4. Influence of Asphalt Binder on the fatigue-life

Table 6. Fatigue Parameters and Models for Asphalt Concrete at Various Binder Content

Asphalt Content %	Intercept	Slope	Models	R^2
4.4	9065.3	0.407	$\mu\varepsilon = 9065.3\ (Nf)^{-0.407}$	0.993
4.9	5424.7	0.319	$\mu\varepsilon = 5424.7\ (Nf)^{-0.319}$	0.983
5.4	4984	0.300	$\mu\varepsilon = 4984\ (Nf)^{-0.3}$	0.973

3.4 Influence of Testing Temperatures on the Fatigue-Life for Asphalt Concrete

Figure 5 exhibits the influence of testing temperatures on the fatigue-life of asphalt concrete. It can be observed

DOI: https://doi.org/10.30564/jbms.v2i2.2792

that the mixture exhibits low fatigue-life when tested at cold environment of 5°C as compared to the warmer environment. This may be attributed to the stiffer condition of the mixture and higher viscosity of the binder. A steep shape of the fatigue-life-microstrain relationship could be detected indicating lower fatigue life and possible brittle and fracture type of failure. On the other hand, the fatigue-life increases significantly as the testing temperature increases regardless of the applied microstrain. For specimens practicing high microstrain level of (750 με), the fatigue life increased by (112.4, and 253.2) % when the testing temperature rises from (5 to 20 and 30) °C respectively. When the asphalt concrete beam specimens were practicing moderate level of microstrain of (400 με), the fatigue life increased by (480.3, and 1370.5) % when the testing temperature rises from (5 to 20 and 30) °C respectively. However, specimens subjected to low microstrain level of (250 με) exhibit an increment in fatigue-life of (1316, and 1588.3) % when the testing temperature rises from (5 to 20 and 30) °C respectively. Such behavior agrees with López-Montero and Miró [7].

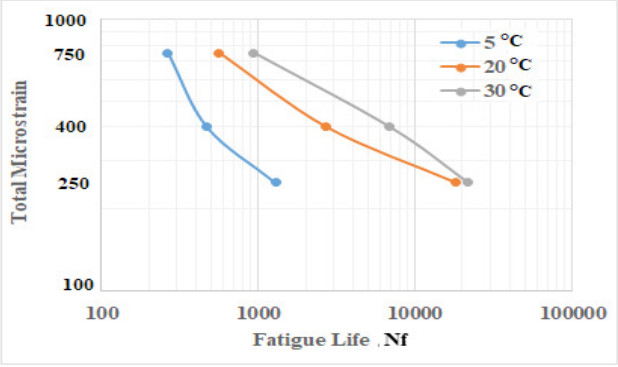

Figure 5. Impact of Testing Temperature on the fatigue-life

Table 7 exhibits the fatigue parameters of asphalt concrete at various testing temperature, it can be noted that increment of testing temperature was able to increase the intercept and decreases the slope, thus exhibiting more flexibility of asphalt concrete. The power models relating the microstrain (με) with the fatigue life (Nf) at various testing temperatures exhibit a strong coefficient of determination (R^2). Similar findings were reported by Quintana and Lizcano [6].

Table 7. Fatigue Parameters and Models for Asphalt Concrete at Various Testing Temperature

Testing Temperature °C	Intercept	Slope	Models	R^2
5	28492	0.669	$\mu\varepsilon = 28492\ (Nf)^{-0.669}$	0.942
20	5214.3	0.314	$\mu\varepsilon = 5214.3\ (Nf)^{-0.314}$	0.981
30	8108.4	0.346	$\mu\varepsilon = 8108.4\ (Nf)^{-0.346}$	0.994

4. Conclusions

According to the testing program and limitations of materials, the conclusions which can be drawn are listed below.

The fatigue-life decreases by (85 and 97) %, (87.5 and 97.4) %, and (71.4 and 95.2) % after increasing the applied microstrain from (250 to 400 and 750) με for control mixture and for mixtures subjected to short-and long-term ageing processes respectively.

The fatigue-life increased by (142.8 and 257.1) %, (34.4 and 57.8) % and (10 and 30) %when the asphalt content increased from 4.4 % to (4.9 and 5.4) % for specimens practicing the applied microstrain of (250, 400 and 750) με respectively.

The fatigue-life increases by a range of (two to fifteen) folds when the testing temperature increased from (5 to 20 and 30)°C respectively.

The developed models could be implemented for prediction of the fatigue-life for asphalt concrete under the assessed conditions.

References

[1] Golchin B. and Mansourian A. (2017). Evaluation of Fatigue Properties of Asphalt Mixtures Containing Reclaimed Asphalt Using Response Surface Method. International Journal of Transportation Engineering, Vol.4, No.4, P. 335-350. Spring.

[2] Song-tao L., Zhaohui L., Juan X. (2015). Fatigue performance of aging asphalt mixtures. Polimery 2015, Vol. 60, No. 2. P. 126-131. Doi: dx.doi.org/10.14314/Polimery. 126.

[3] Glover C. J., Epps Martin E., Chowdhury A., Han R., Prapaitrakul N., Jin X. and Lawrence J. (2009). Evaluation of Binder Aging and Its Influence in Aging of Hot Mix Asphalt Concrete: Literature Review and Experimental Design, Research Report No. FHWA/TX-08/0-6009-1, Texas Transportation Institute, College Station, Texas.

[4] Paul D. K., Sirin O., Kassem E. (2016). Laboratory investigation of asphalt mixture aging. Proceedings, E&E Congress 6th Eurasphalt & Eurobitume Congress, 1-3 June, Prague, Czech Republic.

[5] Al-Khateeb G. and Alqudah O. (2018). Effect of Short-Term and Long-Term Aging on Fatigue Performance of Superpave Hot-Mix Asphalt (HMA). Jordan Journal of Civil Engineering, Volume 12, No. 4. P 580-589.

[6] Quintana H. and Lizcano F. (2012). Evaluation of mechanical parameters of an asphalt mixture under the environmental conditions of Bogotá D.C. Revista

DOI: https://doi.org/10.30564/jbms.v2i2.2792

Ingeniería de Construcción Vol. 27 No1, Abril de 2 www.ricuc.cl.

[7] López-Montero T. and Miró R. (2017). Ageing and temperature effect on the fatigue performance of bituminous mixtures. Materiales de Construcc ión Vol. 67, Issue 327, July-September, e126 http://dx.doi.org/10.3989/mc.2017.04216.

[8] Sol-Sánchez, M.; Moreno-Navarro, F.; García-Travé, G.; Rubio-Gámez, M.C. (2015) Laboratory study of the long-term climatic deterioration of asphalt mixtures. Constr. Build. Mater.88, pp. 32-40. http://dx.doi.org/10.1016/j. conbuildmat.2015.03.090.

[9] Sarsam S. I. (2016). Influence of Aging, Temperature and Moisture Damage on the Stiffness of Asphalt Concrete through the Fatigue Process. International Journal of Scientific Research in Knowledge, 4(4), pp. 077-084. http://dx.doi.org/10.12983/ijsrk-2016-p0077-0084.

[10] Zhu G. J., Wu S. P., Liu R., Zhou L. (2009). Study on the Fatigue Property for Aged Asphalt Mixtures by Using Four Point Bending Tests. Materials Science Forum (Volume 614), March. P. 289-294. https://doi.org/10.4028/www.scientific.net/MSF.614.289.

[11] Miró R., Martínez A., Moreno-Navarro F., Rubio-Gámez M. (2015). Effect of ageing and temperature on the fatigue behavior of bitumen's. Materials & Design, Volume 86, 5 December, P. 129-137. https://doi.org/10.1016/j.matdes.2015.07.076.

[12] Sarsam S. I., AL-Lamy A. K. (2016). Fatigue Behavior of Modified Asphalt Concrete Pavement, Journal of Engineering, 22 (2).

[13] Sarsam S. I., Alwan A. H. (2014). Assessing Fatigue Life of Super pave Asphalt Concrete, American Journal of Civil and Structural Engineering AJCSE 2014, Sciknow Publication, 1(4), pp. 88-95.

[14] Karakas A. S. (2018). Aging Effects on Mechanical Characteristics of Multi- Layer Asphalt Structure. Provisional chapter. http://dx.doi.org/10.5772/intechopen.75698.

[15] SCRB. (2003). State Commission of Roads and Bridges. Standard Specification for Roads & Bridges, Ministry of Housing & Construction, Iraq.

[16] ASTM. (2015). American Society for Testing and Materials. Road and Paving Material, Vehicle-Pavement System, Annual Book of ASTM Standards, Vol.04.03.

[17] AASHTO. (2013). Standard Specification for Transportation Materials and Methods of Sampling and Testing, American Association of State Highway and Transportation Officials, 14th Edition, Part II, Washington, D.C.

[18] . EN 12697-33. (2007). Bituminous Mixtures – Test Methods for Hot Mix Asphalt – part 33: Specimen prepared by Roller Compactor, European Committee for Standardization.

[19] AASHTO. (2013). Standard Practice for Mixture Conditioning of Hot Mix Asphalt (HMA). R30 AASHTO Provisional Standards, American Association of State Highway and Transportation Officials, Washington, D.C.

[20] AASHTO T-321. (2010). Method for Determining the Fatigue Life of Compacted Hot-Mix Asphalt (HMA) Subjected to Repeated Flexural Bending, AASHTO Provisional Standards.

[21] Sarsam S..I, and Alwan A. H. (2014). Impact of Aging on Shear, Tensile Strength and Permanent Deformation of Super pave Asphalt Concrete, International Journal of Scientific Research in Knowledge, 2(10): 487-496.

[22] Sarsam S. I. and AL-Lamy A. K. (2016). Fatigue Behavior of Modified Asphalt Concrete Pavement. Journal of Engineering, Vol. 22 No. 2, February.

 DOI: https://doi.org/10.30564/jbms.v2i2.2792

BILINGUAL PUBLISHING CO.
Pioneer of Global Academics Since 1984

Journal of Building Material Science
https://ojs.bilpublishing.com/index.php/jbms

ARTICLE

Efficient Methodology for Design of Industrial Blast Resistant Electrical Substations and Control Buildings

Osama Bedair*

415-249 Craig Henry Drive, Ottawa, Ontario, Canada

ARTICLE INFO

Article history
Received: 22 February 2021
Accepted: 11 March 2021
Published Online: 30 March 2021

Keywords:
Industrial buildings
Electrical substations
Control building
Steel modules
Analyzer buildings
Steel design
Mobile industrial facilities

ABSTRACT

This paper describes economical strategies to design blast resistant electrical substations and control buildings that are commonly used at industrial plants. Limited literature addressed design aspects for this class of buildings. Furthermore, little guidelines are available in practice to regulate this type of steel construction. The first part of the paper overviews the architectural and structural layouts of electrical buildings. Blast resistance requirements for occupied control buildings are also discussed. Simplified multiple degrees of freedom (MDOF) dynamic model is also illustrated that can be utilized for analysis of the blast resistant buildings. The economical aspects and cost savings resulting in using mobile blast resistant buildings are discussed. The article also highlights the engineering challenges that are encountered in design of mobile electrical facilities. The transportation procedure and design requirements are briefly described. Guidelines are proposed to calculate the center of mass of the building combined with interior equipment. The proposed design concept for electrical and control buildings is cost effective and can be implemented in industry to reduce projects cost.

1. Introduction

Electrical substations, analyzer buildings and control buildings are essential facilities that are required in the operation of industrial plants. These buildings host electrical, instrumentation and mechanical equipment that are required for plants operation. The cost of these buildings is substantial and carful design procedures must be used to economize the design and optimize the capital cost. In surface mining projects, federal and provincial legislations require operators to submit plan showing the restoration of disturbed lands to its original state for future use after completion of mining and oil exploration in order to minimize environmental hazards. Therefore, it is economical to design electrical and control buildings as mobile facilities to be utilized at several locations as the projects expand.

The proposed design concept in order to minimize the project cost is summarized in the flow chart shown in Figure 1. In stage (I), the building is modularized at the fabrication shop. The building at this stage is fully fabricated and commissioned off-site. Instrumentation equipment and electrical cabinets are then installed at the fabrication yard. This approach improves work quality and productivity especially in remote site locations with harsh weather condition, since construction and commissioning are minimized. Furthermore, multidisciplinary work of various activities can be undertaken in parallel. Thus the proposed

**Corresponding Author:*
Osama Bedair,
415-249 Craig Henry Drive, Ottawa, Ontario, Canada;
Email:obedair@gmail.com

DOI: https://doi.org/10.30564/jbms.v2i2.2906

procedure minimizes overall project cost and schedule. In stage (II) the building is transported and delivered to the site as functionally complete unit. The type of transportation vehicle depends upon the overall weight of the building and the access roads to the plant. Furthermore, the modularized building size should not exceed the shipping envelope allowed by the provincial transport regulations. In most cases the envelope is limited to 7.3 m wide x 36 m long x 7.8 m high. Also, the building height should be minimized in order to reduce the material cost. At stage (III) the building is lifted and installed on foundation for a predetermined period of time. At the end of the project duration, the electrical building is decommissioned then jacked and relocated to another plant area, as denoted by Stages (IV) and (V). Note that boxes in the flow chart with green color denote stages that require transportation of the building.

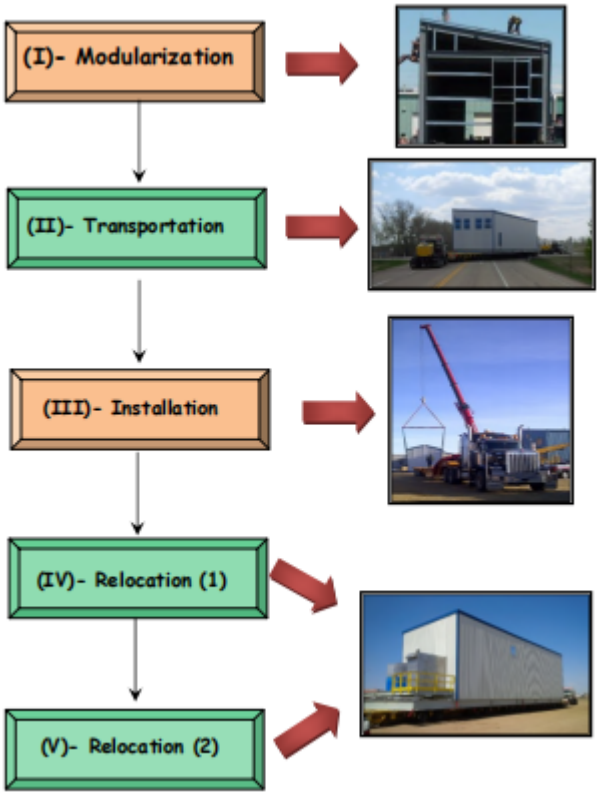

Figure 1. Sequence of Relocating and Installing Mobile Buildings

The engineering phase that would be required by EPC companies to design effective relocation methodology for industrial facilities might take several years depending upon the size and layout of the buildings. It must be noted that failures during relocation of the buildings may result in severe financial losses. Accordingly, proper engineering planning and execution is required to detail the disassembly and re-installation methodologies.

Limited investigations addressed structural design of mobile buildings. Bedair [1-6] presented cost effective procedures for steel fabrication and design of oil&gas and mining facilities. Other studies were conducted to investigate impact of mobile vehicles used in mining projects, e.g. Newman, et al. [7], Burt and Caccetta [8], Alarie and Gamache [9] and Soumis [10]. However, the primary attention was given to mining facilities at permanent locations. Little information is published that address engineering design of mobile structures. Much of the design codes and engineering standards such as AISC [11], AISI [12], ASCE/SEI [13], AASHTO [14], CSA-S136 [15], CSA -S16 [16], NBC [17], Eurocode-3 [18], PIP [19] and Ziemian [20], regulate design of permanent structures.

This paper bridges the gap and provides engineering requirements for design of mobile industrial buildings. The intention is to present cost effective concept for design of mobile buildings that can be utilized in industrial projects. The first part deals with conventional buildings and the second part deals with blast resistant category. The first type is commonly used in non-hazard plant areas while the second type is capable resist petrochemical explosions. The paper also presents a practical multiple degrees of freedom (MDOF) model to determine dynamic response of buildings subjected to far field blast loads. Mathematical derivations to compute displacements and base shear are then presented. The paper provides useful tools that can be used in industry to calculate the dynamic response with little computation effort/cost compared to numerical finite element (FE) method or computational fluid dynamic (CFD) procedures. The described approach can also be used to optimize the building design and reduce project capital costs. It should be emphasized that the scope of the paper is limited to structural and construction aspects. The electrical and instrumentation designs are not covered by this paper.

2. Building Material

There are no general guidelines or rules for the structural material selection in the construction of mobile buildings. Precast concrete panels have been used in several industrial plants. Concrete buildings provide better fire resistance while steel construction provides better ductility and ultimate resistance for seismic and blast loadings. Low carbon steel material exhibits large inelastic strain capacity or deformation ratio. Higher strength steel may not offer sufficient ductility and hence is not economical to use. Concrete has limited ductility and low tensile strength. Furthermore, concrete panels may not be suitable to modularize at fabrication yard or transportation to other site locations.

 DOI: https://doi.org/10.30564/jbms.v2i2.2906

Mobile blast resistant buildings BRB must be capable to absorb and dissipate blast explosion energy while maintaining structural integrity. Building envelope must have adequate ductility and strength to resist lateral loads resulting from blast loads. Therefore, brittle materials such as unreinforced concrete, bricks, timber may not offer adequate blast resistance. In addition, other construction material such as timber or wood could be a fire hazard. Economical design can be achieved by locating the building in a zone with the least blast overpressure without interferences with Electrical or instrumentation functionality. In addition, the building design must utilize the efficient engineering and construction practices.

3. Electrical Building Layout

Electrical buildings envelope is determined according to the interior electrical, instrumentation and mechanical equipment sizes and spacing requirements. Figure 2 shows a typical example for interior layout of electrical buildings. Figure 2a shows rows of vertical electrical cabinets supported by the floor framing. Figure 2b shows suspended cable trays inside an electrical house. Vertical tie rods connected to the main framing are commonly used to support cable trays and are spaced every 6 m. Figure 2c shows vertical instrumentation cabinets that are supported on the side beams.

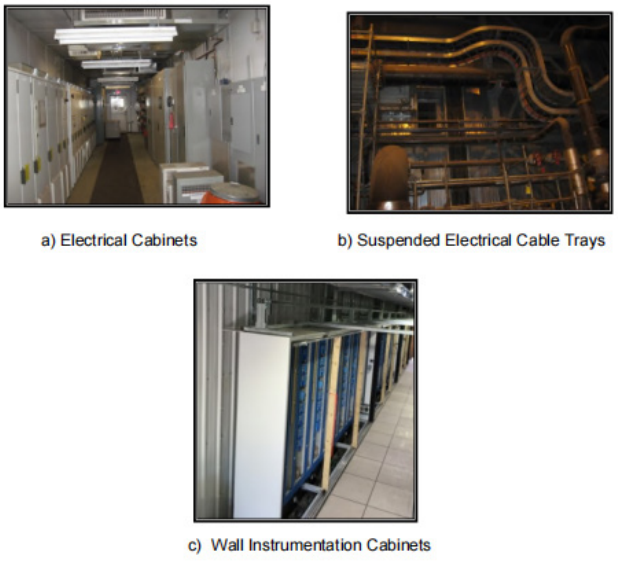

Figure 2. Interior Photos of the Electrical and Control Buildings

Figure 3 shows typical electrical building layout. Relocatable electrical buildings must be supported by steel skid to cope with shipping and transportation requirements. Typical skid layout is shown in Figure 3a.The longitudinal skid beams are bolted to transverse beams that support the floor. The spacing of the transverse beams is determined according to the floor loadings. The skid must be designed to accommodate lifting and transportation loads. Removable or permanent lifting lugs are installed along the columns gridlines. The interior electrical building layout is illustrated in Figure 3b. The primary framing consists of steel columns, inclined rafters, longitudinal and transverse beams as shown by section B-B of Figure 3c. Interior beams across the full width of the building can be used to support electrical cable trays and HVAC ducts as required and shown by electrical/mechanical design drawings. It is recommended to use interior cantilever beam supports at various levels to maximize the useable floor space. The spacing between these supports should not exceed 6 m. Girts and purlins are used to connect external cladding. The building gridlines are located along the column centerlines. It is recommended to use standard 6 m column intervals and vary end bays (as denoted by S in Figure 3b. Building width can be determined based on cabinet number and space requirements. If platforms are attached to the building, they must fall within the transportation envelope. Figure 3d shows side elevation (A) of the building. Side wall penetrations might be provided to allow passage of cable trays to external facilities. However wall penetration should be limited to maximum of 25% of overall wall area.

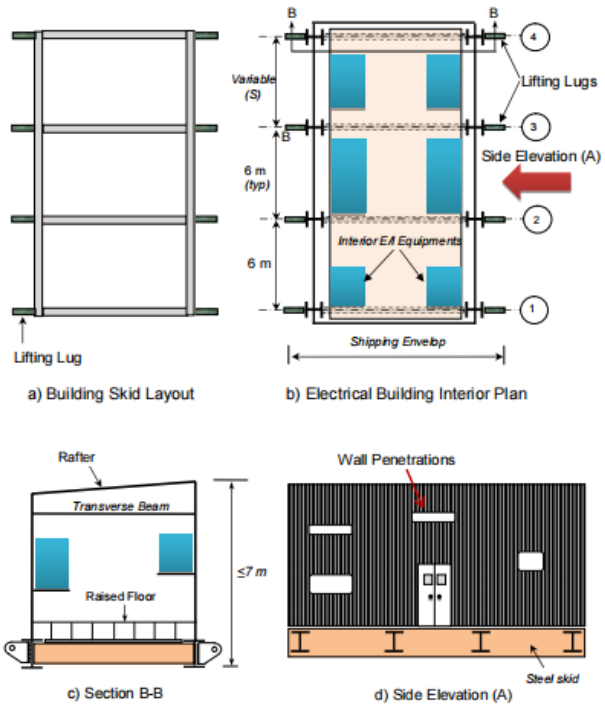

Figure 3. Typical Electrical Building Structural System

DOI: https://doi.org/10.30564/jbms.v2i2.2906

It is also economical from fabrication perspective to use standard member sizes to limit wide variations in steel sections that may result in substantial increase in the building cost. For example, column sizes can be limited to W360 (W14), rafters and perimeter skid beams to W460 (W18), beams and equipment supports to W250 (W10).

Raised floor is provided to meet electrical area classification and installation access to provide under-floor cable tray passage. Figure 4 shows typical raised floor framing layout in electrical buildings. The lower level is used to run cable trays and storage of spare parts. Typical raised floor height is 600 millimeters. Strut sub-frames grids are provided under the cabinets to support the weight. The finished floor is constructed with square, removable, vinyl covered panels using interlocking grid struts.

Figure 4. Raised Floor Framing Layout

4. Firewall and Blast Barriers

Fire requirement shall be determined in accordance with local building codes and in compliance with plant process safety and loss prevention manuals. It is beneficial to use firewalls to protect control buildings or substations adjacent to electrical transformers from fire or explosions. Placement of firewalls is compulsory if the building contains large penetrations. The material of the firewall could be concrete masonry units CMU or galvanized steel panels. The cost of steel panels could be much more expensive than ordinary CMU wall. Other types have recently evolved in the construction market using different material technologies to increase fire-rating. As an example, Figure 5 shows typical layout of firewall arrangement separating electrical building from three external electrical transformers. Section A-A shows the elevation of CMU wall supported by concrete strip footing. Dowel bars are extended from to the foundation to the wall in order to enhance the flexural base capacity. The size and spacing of the dowel bars depend upon the height of the wall.

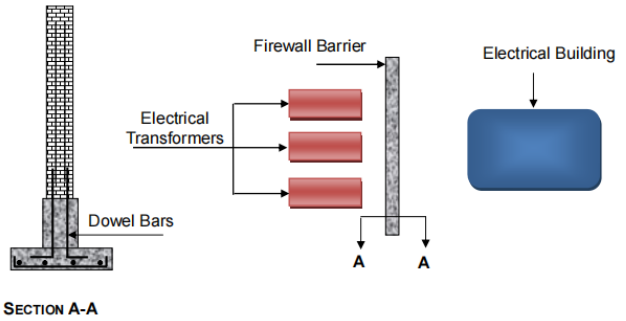

Figure 5. Typical Firewall Barriers

Limited information is available on damage assessments of buildings protected by blast or fire walls. Damage assessment of control buildings due to blast explosions requires accurate prediction of blast loads generation and transfer through the structural members. Little guidelines are also available to predict the reduced level of pressures and impulses behind blast wall. The most popular procedures to calculate blast loadings are based on empirical relationships. The derived equations are developed by assuming no intermediate obstacles between the explosion source and the target. If a blast barrier is used to protect personnel or a structure behind it, the actual blast loading environment will be significantly reduced for some distance behind the barrier. Coughlin, et. al. [21] investigated the response of concrete barriers commonly used to protect essential structures against terrorism actions. Five portable concrete vehicle barriers were tested under satchel sized contact charge explosives. The authors also developed a numerical study using FE method to validate tests data. Other numerical simulation by Remennikov, et al [22, 23] highlighted the effects of adjacent structures on blast loads of buildings located in urban terrain. The authors used neural network-based techniques and experimental data to develop contour plots of overpressure and impulse adjustment factors in order to estimate effectiveness of blast barriers.

5. Mobile Blast Resistant Buildings

Blast resistant buildings BRB are used as shelters to protect personnel working in potentially explosive hazardous areas at industrial plants. Examples of BRB in petrochemical plants are; operator service building, control room, electrical and mechanical buildings, warehouse, administration building, medical and fire stations. The design of these buildings must meet both governing codes and owners safety requirements that are dictated by petroleum industry. Blast resistant buildings BRB are designed as modular steel structures or in some cases or pre-cast concrete. Temporary BRB or trailers are also used during

 DOI: https://doi.org/10.30564/jbms.v2i2.2906

revamp construction projects or turnaround operations to protect people working within process zones in case of explosions.

Blast resistant buildings BRB are critical structures that are used to reduce human fatalities and damages to critical industrial facilities. Mitigation techniques must ensure public safety in the event of accidental explosions. Industrial buildings layout varies significantly depending upon the process design and other engineering disciplines requirements. Complexity in the layout varies from a cubical to major facilities encompassing several buildings. This makes generalized rules for blast resistant design very difficult to achieve. The assessment of blast loading effects on BRB is required during the detailed design phase. The appropriate approach is to perform accurate and reliable evaluation of the blast pressure and impulse acting on the structure. Height of the building should be minimized in order to reduce the cost. The building should be designed using two independent vertical and horizontal resisting systems.

Blast buildings are classified as occupied and non-occupied buildings. Occupied buildings that are located within the process zones such as control rooms, substations, remote I/O building, should be designed as blast resistant buildings in order to maintain operation during explosion or in the post-explosion stage.

5.1 Petrochemical Explosions

Refineries and petrochemical plants have the potential to release clouds of flammable vapor that if ignited produce explosive loads. These explosions results in fast and considerable pressure increase as well as high temperatures. The shock wave propagates with a given speed, magnitude and duration. The properties of gas explosions depend on fuel-oxygen cloud concentration and type of ignition source. Pressure vessel burst is another class of explosion that creates critical hazards at chemical processing facilities. This type of explosions results in both air-blast and fragmentation hazards. The characteristics of blast wave depend upon the vessel geometry. As illustration, side blasts on vessel with cylindrical geometry is stronger than the ends that may create non-circular pressure contours. The directional effects diminish with distance as the expanding shock wave approaches a spherical shape. The U.S Department of Defense [24], published a manual that contains collection of data for explosions related to munitions, manufacturing, handling and storage facilities. Other references such as; American Society of Civil Engineer [25], Canadian Standard Association [26] and Process Industry Practices [27] also provide empirical parameters for general blast loading resulting from bombs, fires and accidental explosions applied to residential and industrial buildings.

The orientation of the building relative to the blast explosion source is critical in determining the magnitude of the blast load intensity on each building side. Figure 6 shows the blast pressure variation (p) with time (t) on the building walls (W_1-W_4). Note that building walls are labeled according to the blast source location. W_1 is wall facing the blast, (W_2&W_3) are the side walls and (W_4) is the rear wall.

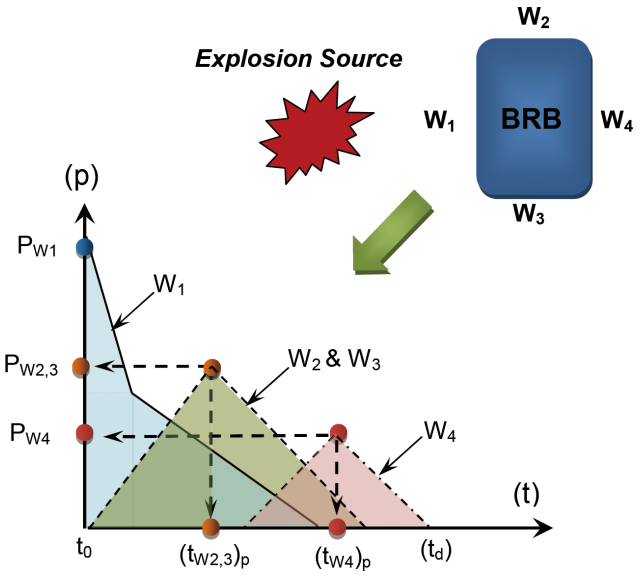

Figure 6. Blas Pressure Variation with Time (t) on Walls (W_1-W_4)

The idealized blast pressure of the wall facing the blast (W_1) is shown by the blue color. The reflected peak overpressure is denoted by (P_{W1}) at time (t)= (t_0). The blast pressure envelop on side walls (W_2&W_3) is shown by the green triangle. Note that side walls (W_2) and (W_3) experience less blast loading compared (W_1) since these walls are not facing the blast. This is due to the gradual loss of blast intensity as the wave travels along the length of the building. The peak pressure on these walls is denoted by ($P_{W2,3}$) at time (t)=$(t_{W2,3})_p$, as shown in Figure 6. As the blast wave reaches the far end of the wall, the overpressure at the near end is reduced. The blast envelop on the rear wall (W_4) is shown by the pink triangle in Figure 6. The peak pressure acting on this wall is reduced to (P_{W4}) at time (t)= $(t_{W4})_p$.

5.2 Simplified MDOF Blast Model

Global dynamic analysis for BRB is required to determine overall peak dynamic displacements and stresses due to application of the blast loads. The common design procedures used in practice for blast resistant buildings BRB

DOI: https://doi.org/10.30564/jbms.v2i2.2906

is simplified by using a single degree of freedom (SDOF) dynamic system. In this approach, the local dynamic response of structural members is determined in isolation. The global response of BRB frame is not determined using (SDOF) model. Therefore, alternative procedure is required to determine the global dynamic response. This section presents multiple degrees of freedom MDOF model that can be used to predict the global dynamic response of BRB.

Consider a typical building shown in Figure 7 exposed to blast explosion. The building contains three rows of electrical cabinets. The explosion source for this building is initiated from the left side as shown. The BRB primary framing consists of steel columns, longitudinal and transverse beams. The column spacing is denoted by (S). Intermediate girders support interior ducts, cable trays and service platforms/catwalks. They also provide lateral restraints to columns and enhance the connection flexibility. The ground elevation GE is measured from the bottom of the steel skid. Raised floor height measured from GE is denoted by (h_1). The separation between the BRB floor and skid floor is approximately (2ft). This spacing is normally utilized to place the cable trays and spare parts. Removable floor panel system is used to facilitate access to the electrical wiring. The skid floor is located on the same elevation as the flange of the skid beams.

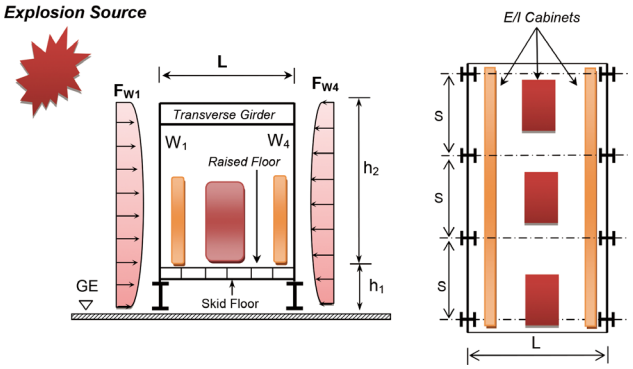

Figure 7. Blast Resistant Building Structural Layout

The idealized structural model is shown is illustrated in Figure 8. The raised floor mass is denoted by (m_1) and is assumed to be uniformly distributed across the width (L). The equivalent floor stiffness is approximated by $(EI_1)_{eqv}$ at floor level (h_1). Dead load at this elevation shall include weight of (EI) cabinets, gas cylinders, cable trays, spare parts, interior ducts and permanent fixtures. The mass and equivalent stiffness at the upper level (h_2) are denoted by (m_2) and $(EI_2)_{eqv}$. Dead load at this elevation shall include suspended cable trays, ducts, elevated equipment and electrical fixtures. The roof and supporting purlins can be included in the calculation of the $(EI_2)_{eqv}$. Note that HVAC units mounted on the roof should be included in the calculation of (m_2).

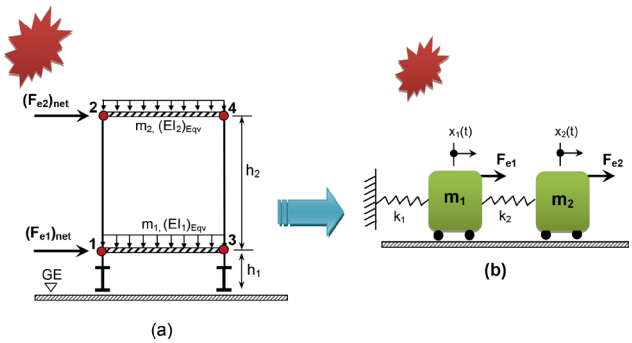

Figure 8. Simplified Equivalent Dynamic (MDOF) Model

Blast design is characterized by impact loads initiated by the blast wave followed by a time dependent pressures that occur due to thermal effects. The net blast forces are lumped at the joints and are approximated as follow:

$$\begin{bmatrix} F_{e1} \\ F_{e2} \end{bmatrix}_{net} = \begin{bmatrix} \left(h_1 + \frac{h_2}{2}\right) & 0 \\ 0 & \frac{h_2}{2} \end{bmatrix} \begin{bmatrix} \left(F_{w1} - F_{w4}\right) \\ \left(F_{w1} - F_{w4}\right) \end{bmatrix} \quad (1)$$

The equivalent two degrees of freedom spring-mass oscillator system is illustrated in Figure 8. Note that $\{x_1(t), x_2(t)\}$ denote the time varying displacement measured from the center of mass. The spring stiffness of each mass are denoted by $\{k_1, k_2\}$, respectively. The governing differential equations are given in the following matrix form:

$$\begin{bmatrix} m_1 & k_1 & -k_2 \\ m_2 & k_2 & 0 \end{bmatrix} \begin{bmatrix} \ddot{x_1}(t) & \ddot{x_2}(t) \\ x_1(t) & \left[x_2(t) - x_1(t)\right] \\ \left[x_2(t) - x_1(t)\right] & 0 \end{bmatrix} = \begin{bmatrix} F_{e1}(t) \\ F_{e2}(t) \end{bmatrix} \quad (2)$$

Where $\ddot{x_i}(t)$ and $\dot{x_i}(t)$ are the acceleration velocity of the idealized mass due to blast loading.

The natural frequency of the building frame is determined by setting the right hand sides of Equation (2) to zero. For this condition, the system undergoes free vibration. The non-trivial solution is obtained by setting the determinant of the coefficient to zero. This yields the following characteristic equation:

$$\begin{bmatrix} \omega^4 & \omega^2 & 1 \end{bmatrix} \begin{bmatrix} 1 \\ -\delta \\ \beta \end{bmatrix} = 0 \quad (3)$$

Where:

$$\delta = \left(\frac{k_1 + k_2}{m_1} + \frac{k_2}{m_2} \right), \quad \beta = \frac{k_1 k_2}{m_1 m_2} \tag{4}$$

The natural frequency of the structure is solution of Eq. (3) and is given by:

$$\omega_1 = \sqrt{\frac{1}{2}\left(\delta - \sqrt{\delta^2 - 4\beta} \right)}, \quad \omega_2 = \sqrt{\frac{1}{2}\left(\delta + \sqrt{\delta^2 - 4\beta} \right)} \tag{5}$$

The corresponding natural period $\{T_1, T_2\}$ are given by:

$$T_1 = \frac{2\pi}{\omega_1}, \quad T_2 = \frac{2\pi}{\omega_2} \tag{6}$$

Determination of the building response due to blast loading requires the solution of coupled differential Eq. (2) that can be transformed into system of uncoupled equations by expressing the solution in form of generalized functions z(t) with normal or orthogonal modes as follow:

$$\begin{bmatrix} x_1(t) \\ x_2(t) \end{bmatrix} = \begin{bmatrix} a_{11} & a_{12} \\ a_{21} & a_{22} \end{bmatrix} \begin{bmatrix} z_1(t) \\ z_2(t) \end{bmatrix} \tag{7}$$

Where $\{z_1(t), z_2(t)\}$ are orthogonal time varying functions that describe vibration mode subject to blast excitation and $\{a_{ij}\}$ are the associated coefficients that determine the contribution of each mode. Substituting these functions into Eq.(2) results into the following normalized differential equations

$$\begin{bmatrix} z_1^{\bullet\bullet}(t) & z_1 \\ z_2^{\bullet\bullet}(t) & z_2 \end{bmatrix} \begin{bmatrix} 1 & 1 \\ \omega_1^2 & \omega_2^2 \end{bmatrix} = \begin{bmatrix} P_1(t) \\ P_2(t) \end{bmatrix} \tag{8}$$

Where:

$$\begin{bmatrix} P_1(t) \\ P_1(t) \end{bmatrix} = \begin{bmatrix} \varphi_{11} & \varphi_{12} \\ \varphi_{21} & \varphi_{22} \end{bmatrix} \begin{bmatrix} F_{e1}(t) \\ F_{e2}(t) \end{bmatrix}_{net} \tag{9}$$

Where (φ_{ij}) denote the normalized vibration modes that are described by the following compacted form:

$$\varphi_{ij} = \frac{a_{ij}}{\sqrt{\sum_{k=1}^{n} m_k \, a_{kj}^2}} \tag{10}$$

The solution of the uncoupled differential Eq. (8) can be obtained numerically to determine the displacement profile. An upper limit for the maximum response can be obtained by adding the absolute values of the maximum modal contributions. This can be attained by replacing $\{z_1, z_2\}$ by $\{z_{1max}, z_{2max}\}$ and adding the absolute values, as follow:

$$\begin{bmatrix} y_{1\max} \\ y_{2\max} \end{bmatrix} = \begin{bmatrix} \varphi_{11} & \varphi_{12} \\ \varphi_{21} & \varphi_{22} \end{bmatrix} \begin{bmatrix} |z_1(t)| \\ |z_2(t)| \end{bmatrix}_{\max} \tag{11}$$

Equation (11) provides an upper limit to the maximum response at joints (1) and (2) of Figure 8. Determination of (z_{1max}) and (z_{2max}) can be determined from the following relation:

$$\begin{bmatrix} z_1(t) \\ z_2(t) \end{bmatrix}_{max} = \begin{bmatrix} DLF_1 & 0 \\ 0 & DLF_2 \end{bmatrix} \begin{bmatrix} z_1(t) \\ z_2(t) \end{bmatrix}_{Static} \tag{12}$$

where (DLF_1) and (DLF_2) are dynamic load factors. The displacements $\{(Z_1)_{static}, (Z_2)_{static}\}$ are determined from:

$$(z_1)_{Static} = \frac{P_1(t)}{\omega_1^2}, \quad (z_2)_{Static} = \frac{P_2(t)}{\omega_2^2} \tag{13}$$

Alternatively, the square root of the sum of the squares of the modal contributions provides reasonable approximation to the maximum displacement as follows:

$$\begin{bmatrix} y_1^2 \\ y_2^2 \end{bmatrix}_{\max} = \begin{bmatrix} \varphi_{11}^2 & \varphi_{12}^2 & 0 & 0 \\ 0 & 0 & \varphi_{21}^2 & \varphi_{22}^2 \end{bmatrix} \begin{bmatrix} z_1^2(t) \\ z_2^2(t) \\ z_1^2(t) \\ z_2^2(t) \end{bmatrix}_{\max} \tag{14}$$

Having determined the maximum dynamic displacements and associated modal shapes, the maximum column shear forces under blast loading can be determined using the following;

$$V_{ij} = z_{j\max} \left(\varphi_{ij} - \varphi_{i-1,j} \right) \quad k_i \tag{15}$$

Equation (15) can be expanded for the idealized model as follows:

$$\begin{bmatrix} V_{11} \\ V_{12} \\ V_{21} \\ V_{22} \end{bmatrix} = \begin{bmatrix} (\varphi_{11})_{k_1} & 0 & 0 & 0 \\ 0 & (\varphi_{12})_{k_1} & 0 & 0 \\ 0 & 0 & (\varphi_{21} - \varphi_{21})_{k_2} & 0 \\ 0 & 0 & 0 & (\varphi_{22} - \varphi_{12})_{k_2} \end{bmatrix} \begin{bmatrix} z_1(t) \\ z_1(t) \\ z_2(t) \\ z_2(t) \end{bmatrix}_{\max} \tag{16}$$

The maximum shear forces are obtained from:

DOI: https://doi.org/10.30564/jbms.v2i2.2906

$$\begin{bmatrix} V_1^2 \\ V_2^2 \end{bmatrix}_{\max} = \begin{bmatrix} V_{11} & V_{12} \\ V_{21} & V_{22} \end{bmatrix} \begin{bmatrix} V_{11} & V_{21} \\ V_{12} & V_{22} \end{bmatrix} \quad (17)$$

To illustrate the procedure numerically, assume it is required to determine for the building frame shown in Figure 8 the maximum displacements and base shear forces. The building parameters are (h_1)= 6 ft, (h_2)= 15 ft and (L)=30 ft. The column size is W10x45. The equivalent floor stiffness $(EI_1)_{eqv}$ = 7.44x10^9 Ib-in^2 and $(EI_2)_{eqv}$ = 3.2x10^9 Ib-in^2. Total first level floor load (P_1) =52 kip and the second level is (P_2)= 25.5 kip. The blast load at the joints are $(F_{e1})_{net}$=10 kip and $(F_{e2})_{net}$ =20 kip. Blast duration (t_d)= 0.1 sec. The non-dimensional parameters are (δ) = 3825, (β) = 701,874. Accordingly, the building natural frequency parameters are (ω_1) = 13.9 rad/s and (ω_2) = 60.26 rad/s. The natural periods are determined as (T_1) = 0.45 sec and (T_2) = 0.1 sec. The dynamic load factors are therefore $(DLF_1)_{max}$=0.57 and $(DLF_1)_{max}$=1.22. The maximum sway deflection $(y_2)_{Max}$ = 0.9 in. Maximum base shear of the building can be computed using Eq.(16) as $(V_1)_{max}$ = 8.04 kip and $(V_2)_{max}$ = 5.80 kip. Accordingly, the total base shear (V_{total}) =13.84 kip

5.3 Global Response Limits

Performance criteria specify the limits on the dynamic response for (BRB) in order to achieve blast design objectives. Generally, the more deformation the building component is able to undergo without failure, the more blast energy that can be absorbed. In blast dynamic analysis, the structural response is governed by the member ductility. Therefore, response limits are typically placed on the maximum dynamic deflection.

Damage classification currently used in the industry provides high level global definition for building response. The common performance or response criteria used for (BRB) are; a) Low Response; b) Moderate Response and c) High Response. In category (a) localized building damage is allowed. In category (b) larger or widespread damage is allowed. In category (c) severe global damage or collapse is permitted in the post blast event.

Table 1 provides recommendations to maximum dynamic sway deflection for the three performance criteria. Overall building height measured from the ground elevation (GE) is denoted by (H)=(h_1+h_2). The maximum sway should not exceed (2%) for buildings designed for low response. These limits are increased to (4%) for high response.

Table 1. Proposed Sway Deflection Limits for BRB

Sway Deflection Limits	Low Response	Medium Response	High Response
	H/50	H/35	H/25

6. Foundation Systems

Several foundation systems can be used to support mobile industrial buildings. Figure 9 shows two possible foundation schemes that can be used to support mobile buildings. If the soil bearing capacity is adequate, the foundation system option (I) shown in Figure 9a can be used. The building in this case is placed on mat foundation with concrete pedestals projected to the predetermined installation elevation, as shown in Figure 9a. The longitudinal skid beams are anchored to the concrete pedestals. Fixed or pinned boundary conditions can be used to stimulate the connection to the foundation.

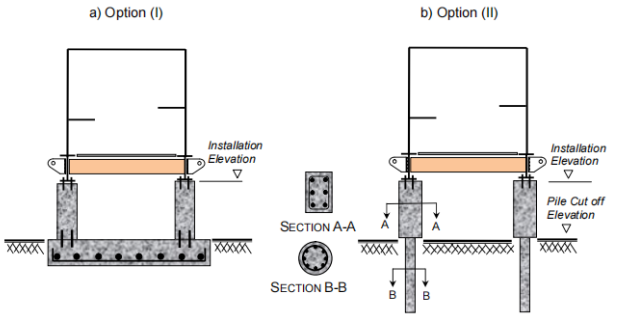

Figure 9. Support System

Figure 9b shows alternative foundation option (II) that can be used for weak soil conditions. Rectangular or circular concrete pedestals can be used, in this case, to support the electrical building. The pedestals are projected from the underground piles at the cut-off up to the installation elevation. Section A-A of Figure 9b shows typical reinforced rectangular concrete pedestal and section B-B shows typical circular pile section. Determination of pile size and length should be based upon the soil characteristics and geotechnical recommendations. If the stiffness of the hard soil stratum is not adequate to provide fixed end bearing to the pile base, vertical restraints must be used in structural analysis model. In this case, pile capacities are estimated by combining skin friction resistance and soil end bearing.

7. Transportation Vehicles

It is recommended to use Self Propelled Module Trailer (SPMT) to transport industrial facilities located on irregular terrains. The vehicle contains a computer system that monitors and controls the motion of the substation during transportation. A schematic of typical SPMT plan and elevation is illustrated in Figure 10. The platform width is 2.43 m and the length can be variable depending upon the number of axel lines used. For example, SPMT platform length of the using six axle lines is 8.4m,

DOI: https://doi.org/10.30564/jbms.v2i2.2906

as shown in Figure 10. Each wheel in the SPMT adjust independently to allow it to turn or even spin in place, to make it possible to adjust the SPMT`s directions accurately. During transportation, the hydraulic rams allow the SPMT wheels to telescope independently so that the structure is kept flat while moving over uneven or sloped roads. This feature keeps the load distribution on each wheel unchanged, and minimizes the possibility of sliding when driving over slopping surfaces. The operating SPMT speed ranges between 3-5 km/hr can be adjusted as required.

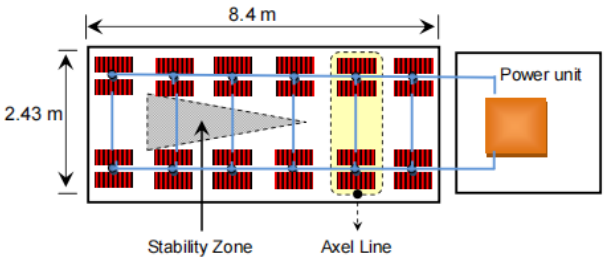

Figure 10. SPMT Vehicle Layout

The center of mass for the transported structure must be located within the triangular stability zone. The coordinates of the triangular stability zone of the SPMT is determined by the manufacture specifications and must be provided prior to relocation. For large electrical substations, several SPMT's trailers are coupled side to side or end to end to match the facility configuration and engineering requirements. The coordinates of the stability zone for the assembled SPMT's varies and depends upon the trailers layout. It must be noted that alignment of substation center of mass within SPMT's stability zone is a challenging task that must be addressed during relocation design cycle.

8. Impact Load Factors

Modularization of industrial buildings is a cost effective procedure that results into to significant savings. However, major disadvantages in using modular buildings are the increase in the engineering activities and material cost. The substation modules are required to be designed for lifting and transportation conditions which require using heavier steel sections. This increase in the steel quantity is estimated to be around 40%. Impact loads induced during transportation and lifting should be considered in addition to the operational conditions. Equivalent static analysis procedure can be used to approximate the induced impact loads during transportation.

Lifting details of typical modularized building are shown in Figure 11a. Four or eight lifting points can be used depending upon the building size. The steel skid must be designed to accommodate lifting loads with an appropriate factor of safety. It is recommended to use removable lifting lugs as shown in Figure 11b. Lifting lugs are installed on the longitudinal beam webs along the column grids using end plate bolted connections. It is also recommended to use the same connection type for the transverse beams. Reinforcing plates (shown in detail E) might be required to be welded around the lifting lug hole on both sides to enhance stiffness at the stress concentration regions. The lifting lugs should be designed according to the shackle capacity used by the lifting crane. The size of the lifting hole must match the lifting pin size. Also the edge distance must be sufficient to prevent failures. The lifting lugs must be checked against combined tension and shear block failures using design factor of safety 5. The connecting bolts should also be checked against combined shear and tension failures.

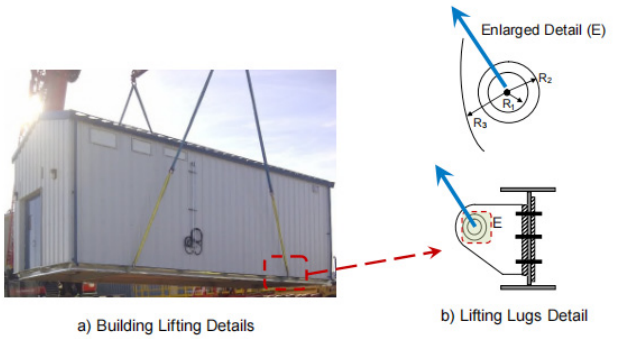

Figure 11. Illustration of Lifting Details of modular Building

9. Jacking of Electrical Buildings

Hydraulic jacking can be used to relocate existing mobile buildings at the end of the project. The buildings are first decommissioned and disassembled from the existing foundation at the original location, then transported to re-use at the new plant location. Therefore, the building is required to be designed for upward jacking as well. Figure 12 illustrates schematically the overall procedure. SPMT trailers with adjustable platforms are first placed between the concrete pedestals. Then hydraulic jacking can be used to raise the base frame support up to the desired elevation. This step becomes very complicated if the building contains heavy equipments or composed of several units. Also un-symmetric distribution of mass within the facility may offset the centre of mass (CM) and complicates jacking procedure and transporting vehicle layout.

DOI: https://doi.org/10.30564/jbms.v2i2.2906

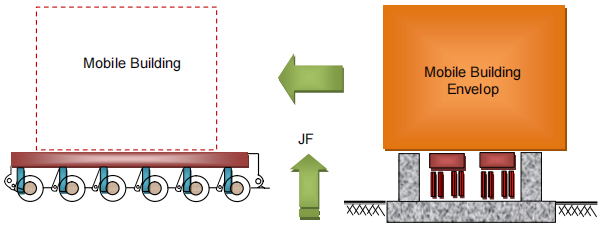

Figure 12. Jacking and Relocation of Electrical Substation

Upward jacking of electrical substation is accomplished using hydraulic stool system. The magnitude of the jacking forces (JF) is determined by the construction contractors based on weight and combined centre of mass location. Accurate calculation of combined (CM) coordinates is very critical and must be computed accurately to avoid failures during jacking or transportation. Engineering models must be developed prior to execution. Therefore, the magnitude of the jacking forces used by the construction contractor must be provided to the design engineer prior to execution. The computation of the center of mass (CM) for the transported electrical substations must include structural steel members, mechanical and electrical equipment, cable trays and electrical cabinets.

10. Design Guidelines

The initial building model is normally developed by several disciplines during the front end engineering phase. The model should be tested against critical load conditions including operation, lifting, jacking and transportation cases. The structural model must be continuously updated prior to execution and tested for serviceability and ultimate limit states (SLS and ULS) for disassembly, transportation, and installation. Structural stability of the building should be examined and peak dynamic displacements shall be determined by accounting for material non-linearity and P-Δ effect.

Structural components of mobile building shall be designed for strength and serviceability limit states in accordance to local codes requirements. Members should be checked with each type of loading in order to determine the most severe load condition. Interior equipment connections must also be examined for relocation. It must be noted that some vendors designs may not account for the impact forces induced during relocation. The engineer should also explore possible options to reinforcing weak connections or critical members. The structural model update must also include the new members or structural reinforcements.

Sub-models are then generated to examine the structural serviceability ultimate limit states (SLS &ULS). It must be noted that the boundary conditions and applied loads that are used in these models are different. The engineer must verify (SLS) and (ULS) during the jacking and disassembly procedures. Temporary supports that will be used during the jacking procedure must also be incorporated in this model. Determination and points of applications of the impact factors during the jacking is also very essential. The engineer must idealize points of contact between the structural framing and the jacking stools.

The transportation roads that will be used by the SPMT's must also be inspected prior to mobilization. Soil strength in some projects may not be capable to sustain the combined SPMT and the structure. Survey to the existing slopes must be performed to identify the profile changes following several years of operation. It must be noted that in many project sites transportation rods are constructed using compacted layers of gravel, and the changes in the road profile or condition are very common. Obstructions to the SPMT's manoeuvres must also be identified.

The engineer must also examine structural (SLS) and (ULS) during lifting and installation procedures. Artificial boundary conditions might be required to stabilize the structural analysis model. Appropriate safety factors must be used during the crane lifting and installation.

11. Conclusions

This paper presented economical concepts for design of electrical substations and control buildings. Limited literature and guidelines are available in practice for various design aspects for this class of buildings. The paper overviewed the structural layouts of typical electrical substations. The economical aspects and cost savings resulting in using relocatable electrical buildings were also discussed. The paper also highlighted various engineering challenges that are encountered in the design of mobile industrial facilities. The transportation procedure and design requirements were briefly described. Recommendations were provided to compute the combined center of mass of the substation and interior equipment. Effective analysis procedure is also described. The proposed design concept for mobile buildings is cost effective and can be implemented in industry to reduce projects cost.

Current building codes are not adequate for design of BRB. Additional guidelines and design provisions are required to accurately define blast loading parameters and set limitations on BRB dynamic response. Unfor-

 DOI: https://doi.org/10.30564/jbms.v2i2.2906

tunately, little design rules are available in practice for this class of buildings that are extensively used in the industry. The paper presented MDOF dynamic model to evaluate dynamic response of industrial BRB. The loading conditions and structural design criteria of BRB were briefly described. The mathematical derivations to compute the global displacement and base shear were presented. Building example was then provided to illustrate the computation procedure. The paper provides useful tools that can be used in industry to calculate BRB dynamic response with little computation effort compared to numerical FE or CFD models. Structural response can be calculated manually using formulas of section (5.2).

Effective BRB structural system should be capable to absorb and dissipate the blast explosion energy while maintaining the structural integrity. The building must have adequate ductility and strength to resist lateral loads resulting from the blast wave. The limits of Table 1 can be used as guidance to define the level of damage acceptable for blast resistant building.

Damage classification procedures used in the industry for BRB are not economical since it is based on the overall building response. For example, local failures BRB is not permitted for secondary members. Therefore, it is more economical to establish alternative local damage classification procedure. It is also recommended to standardize the design of BRB according to the magnitude of blast pressure and impulse duration.

References

[1] Bedair, O. (2020), “Economical Damage Classification Procedure for Blast Resistant Buildings in Petrochemical Plants”, ASCE, Practice Periodical on Structural Design and Construction,25(3),04020020.

[2] Bedair, O. (2015) "Novel Design Procedures For Rectangular Hollow Steel Sections (RHSS) Subject To Compression, Major & Minor Axes Bending", ASCE, Practice Periodical on Structural Design and Construction , 20, 04014051.

[3] Bedair, O. (2014) “Cost Effective Modularization Strategies for Industrial Facilities Used in Mega Oil&Gas Projects" Recent Patents on Engineering, 8, pp.120-132.

[4] Bedair,O. (2014) “Rational Design of Pip-Racks Used For Oil Sands and Petrochemical Facilities", ASCE, Periodical on Structural Design and Construction, 20 (2), 04014029.

[5] Bedair, O. (2014) “Modern Steel Design and Construction Used In Canada's Oil Sands Industry" Journal of Steel Design Construction and Research", 7 (1), pp.32-40.

[6] Bedair, O. (2012) “Interaction of Multiple Pipe Penetrations Used In Mining and Petrochemical Facilities”, Journal of Thin-Walled Structures, 52, 158-164.

[7] Newman, A. M., Rubio, E., Caro, R., Weintraub, A., and Eurek, K. (2010) "A review of operations research in mine planning" Interfaces, 40(3), 222-245.

[8] Burt, C. & Caccetta, L. (2007) "Match factor for heterogeneous truck and loader fleets", International Journal of Mining, Reclamation and Environment, 21(4), 262-270.

[9] Alarie, S, and Gamache, M. (2002) "Overview of solution strategies used in truck dispatching systems for open pit mines",International Journal of Surface Mining, Reclamation and Environment, 16(1),59-76.

[10] Soumis, F., Ethier, J., and Elbrond (1989) "Truck dispatching in an open pit mine. International", Journal of Surface Mining Reclamation and Environment, 3(2), 115-119.

[11] AISC (2006), “Steel Construction Manual”, 14th Edition. American Institute of Steel Construction, Chicago, USA.

[12] AISI (2007), “North American Specification for the Design of Cold-Formed Steel Structural Members”, American Iron Steel Institute, Washington DC, USA.

[13] ASCE/SEI 7-10 7 (2010) "Minimum Design Loads and other structures", American Society of Civil Engineers, Virginia, USA.

[14] AASHTO LRFD Bridge Design Specifications, (2012) American Association of State Highway and Transportation “- Customary US units “ AASTO Publications, Washington.

[15] CAN/CSA-S136-07 (2007) ” North American Specification for the Design of Cold-Formed Steel Structural Members”, Canadian Standard Steel Association, Mississauga, Ontario.

[16] CAN/CSA-S16-01 (2010) “Limit states design of steel structures”, Canadian Standards Association, Mississauga, Ontario, Canada.

[17] NRC (National Research Council of Canada). 2010. National building code. Ottawa, ON: National Research Council of Canada.

[18] Eurocode 3: (2005) Design of steel structures Part 1.5: plated structural elements; EN 1993-1-5: 2005.

[19] Process Industry Practices-PIP STC01015, (2014) "Structural design Criteria", Texas, USA.

[20] Ziemian, R. (2010) “Guide to Stability Design Criteria for Metal Structures”, 6th edition, John Wiley

DOI: https://doi.org/10.30564/jbms.v2i2.2906

and Sons Ltd.

[21] Coughlin AM, Musselman ES, Schokker AJ, Linzell DG. (2010) " Behavior of portable fiber reinforced concrete vehicle barriers subject to blasts from contact charges" International Journal of Impact Engineering; 37(5): 521-529.

[22] Remennikov AM. (2003) A review of methods for predicting bomb blast effects on buildings. J Battlefield Technol 6(3):5-10.

[23] Remennikov AM, Rose TA. (2005) Modelling blast loads on buildings in complex city geometries. Int J Comput Struct;83, 2197-2205.

[24] US Army Corps of Engineers TM 5-1300 (1990) "Structures To Resist The Effects Of Accidental Explosions", New York, USA.

[25] ASCE (2010) "Design of Blast Resistant Buildings in Petrochemical Facilities" ASCE Petrochemical Committee, Task Committee on Blast Resistant Design, New York.

[26] CSA S850-12, (2017) "Design and Assessment of Buildings Subjected to Blast Loads" Canadian Standard association, Toronto, Canada.

[27] Process Industry Practices PIP STC 01018 (2014) "Blast Resistant Building Design Criteria", USA.

 DOI: https://doi.org/10.30564/jbms.v2i2.2906

BILINGUAL PUBLISHING CO.
Pioneer of Global Academics Since 1984

Journal of Building Material Science
https://ojs.bilpublishing.com/index.php/jbms

REVIEW

Perspective of E-Waste in Concrete: A Review

Kiran Devi* **Amit Kumar**

Civil Engineering Department, National Institute of Technology, Kurukshetra, 136119, India

ARTICLE INFO

Article history
Received: 30 December 2020
Accepted: 2 March 2021
Published Online:30 March 2021

Keywords:
E-waste
Cement composites
Bituminous mix
Properties of concrete

ABSTRACT

In this digital era, usage of electric and electronic devices has become the need of people. Evolution of technology triggers the adoption of new devices over old and discarded appliances turned into the electronic wastes also termed as e-waste/s. E-waste from any source has become a major concern to the society. The disposal of these wastes into the landfills causes many hazardous impacts to the ecosystem. As a promising solution construction industry can utilize the e-wastes effectively. The wastes may be used either as fine filler or aggregates in concrete and bituminous based constructions efficiently. Usage of waste/s conserves the natural resources also. Present study magnifies the scenario of application of electronic wastes in different forms i.e., plastic, metal etc. in bituminous and concrete based mixtures. A critical review has been carried the effects of electronic wastes in concrete and bituminous mixes and findings confirm the praxis of electronic wastes is possible within certain limits.

1. Introduction

Advancement in technology pushes the use/dependence of electric and electronic appliances i.e., computer, mobile, television, refrigerator etc. in day-to-day life and use to people can switch to advanced devices very easily at affordable prices. Obsoleted old devices turn into the e-waste and also increasing along with the production/manufacturing of new devices at rumoring speed globally [1].

In 2018, 50 MT of electronic wastes (e-wastes) was generated globally and half of this related to personal devices i.e., computers, monitors, chargers, screens, smart phones, motherboards, tablets and TVs etc. while rest were the large household appliances i.e., comfort equipments. Figure 1 depicts the sources of e-waste. According to a study, only 20% of global e-waste is recycled per annum i.e. 40 million tonnes of e-waste is dumped in landfill, burned or illegally traded and treated in a substandard way. As the land is precious resource, therefore it should be conserved rather than dumped every waste into it. In India, e-waste in the form of computer along its devices, telecommunication, electricity and medical equipment and household scraps is generated. Mumbai is the leading city in waste generators followed by Delhi, Bangalore, Chennai and Kolkata [2].

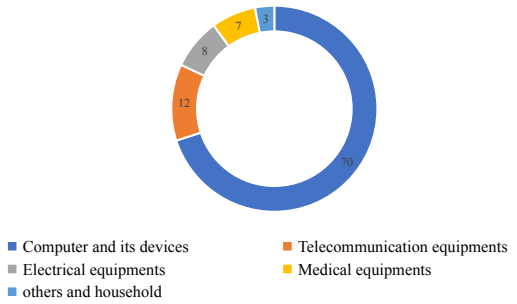

Figure 1. E-wastes generation from different sources [2]

**Corresponding Author:*
Kiran Devi,
Civil Engineering Department, National Institute of Technology, Kurukshetra, 136119, India;
Email: kiranbimbhra@gmail.com

DOI: https://doi.org/10.30564/jbms.v2i2.2759

In electronic wastes, there are more than thousand different types of toxic elements i.e. lead, mercury, cadmium etc. The ferrous metal, non-ferrous metal, glass, plastics and others are present in e-waste. The percentage of materials in electronic wastes has been shown in Figure 2. Approximately 20 to 50 million tonnes of e-wastes are discarded globally and 12 million were from Asia only (178million in China and 80 million in India of total 716 million computer users globally). In 2016, 44.7 million metric tonnes of e-waste were generated which is equal to almost 4500 Eiffel towers. Every year 20-25 million tonnes of e-waste are generated globally. The expected generation of e-wastes year-wise has been shown in Figure 3. In India, 2 million metric tonnes of e-waste are generated in 2016 [3].

Natural resources are deteriorating at a faster rate due to technological development, changes in consumption habits and rapid population growth. The wastes like plastic, industrial wastes, agricultural wastes, medical wastes, construction & demolition wastes and organic or electronic wastes are generating with the growth of industrialisation. Like all wastes, the generation of electronic wastes is increasing globally due to consumption of electrical and electronic devices with the advancement in information technology. The usages life of these devices has been shortened. Therefore, the e-wastes have emerged as fast-growing solid wastes in various dimensions [4-6].

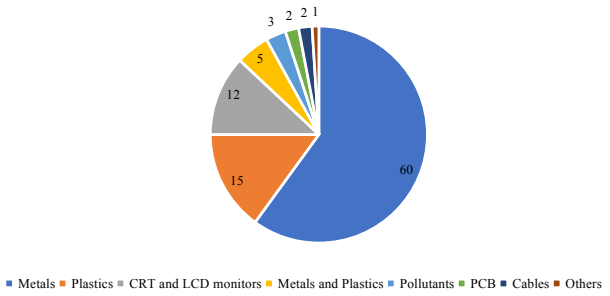

Figure 2. Materials in e-wastes (%) [3]

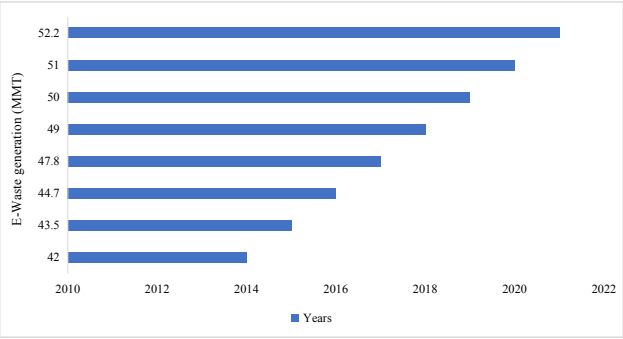

Figure 3. Year-wise generation of e-wastes (Needhidasan and Agarwal, 2019)

Approximately 40 million tons e-wastes were generated globally in 2015 and it increased to 47 million tons in 2017. But, only 10% of e-wastes is safely recycled and the rest is disposed of either in landfills, burned in incinerators or shipped to developing countries where rudimentary recycling of e-wastes takes place. Electronic waste is complex and consists of valuable i.e. metals and renewable materials as well as toxic or harmful elements i.e. plastic, liquid crystal and organic matter. The improper handling or disposal of e-wastes causes serious environmental pollution and threat to human health. This recent situation demands for recycling of wastes safely. The methods and technologies used in the recycling of e-wastes are very different from that of minerals. The recycling of e-wastes is more complex as compared to minerals. The techniques include physical separation, pyrometallurgical technology, mild extraction technology, electrochemical technology and vacuum metallurgical technology are the economical and eco-friendly; and recycles valuable resources effectively [7].

The disposal of huge quantity of e-waste plastic cause serious issue to ecosystem due to low biodegradability. The reuse of e-waste plastic either as fine aggregates (FA)/coarse aggregates (CA) or filler in the concrete or pavement construction not only lower the cost but also solve the huge disposal problems. A possible and feasible solution of e-waste is harnessed in the construction industry. In the present study, the effect of electronic wastes of various forms in bituminous or concrete mixes construction has been reviewed. The various properties of cement composites containing electronic waste i.e. workability, compressive strength (CS), split tensile strength (STS), flexural strength (FS), chemical resistance, chloride ion permeability etc. have been studied and reviewed.

2. Literature Review

The e-waste has been used in concrete and pavement construction as partial substitution to naturals resources. The effects of partial replacement of raw materials by e-wastes in bituminous and concrete mixes have been given in Table 1 and 2 respectively.

2.1 Bituminous Construction

Increase in e-waste plastic reduced the ductility gradually and increased the penetration value, viscosity and softening point. E-waste plastic powder at 10% can be used for the road pavement [8] as given in Table 1. Increase in e-waste powder in bitumen increased the penetration value, softening point, flash and fire point, viscosity, specific gravity and decreased the ductility value. Modified bitumen had higher stability value [9].

DOI: https://doi.org/10.30564/jbms.v2i2.2759

2.2 Concrete Construction

Table 2 showed the effect of e-wastes in the cement composites on the various fresh properties and hardened properties and discussed as below.

2.2.1 Fresh Properties

10% e-waste slump value increased afterward it decreased (S, 2020). Waste PCB increased the air content and water retention property and decreased the bulk density of mortar [10]. The workability of concrete decreased with the increase in e-plastic waste due to its hydrophobic nature and its rough surface and angular shape result into increase in inner friction and reduced flow [11, 12, 14, 18, 19, 26].

Table 1. E-waste in bituminous mix

References	Waste (%)	Conclusions
Santhanam et al., 2019 [8]	E-waste plastic as aggregate at 5%, 10% and 15%	Increase in e-waste plastic reduced the ductility gradually and increased the penetration value, viscosity and softening point. E-waste plastic powder at 10% can be used for the road pavement.
Kumar et al., 2020 [9]	Electronic circuit boards (E-PCB) in the form of fine powder 0%, 6%, 12% & 18% and non-metallic chips at 0%, 5%, 10% and 15%	Increase in e-waste powder in bitumen increased the penetration value, softening point, flash and fire point, viscosity, specific gravity and decreased the ductility value. Modified bitumen had higher stability value.

Table 2. Cement composites consisting e-waste

Authors	Wastes	Results
Wang et al., 2012 [10]	Waste printed circuit boards non-metallic powder (PCB) as admixture	Waste PCB increased the air content and water retention property but decreased the bulk density of mortar. Waste PCB less than 15% did not decreased CS and FS rapidly afterward it decreased gradually.
Kumar and Baskar, 2015 [11]	E-plastic waste as CA (10%, 20%, 30%, 40% and 50%)	The workability and density of concrete decreased with the increase in e-plastic waste. The addition of e-plastic waste lowered the CS and FS and had high deformability behaviour before failure.
BT, 2016 [12]	E-plastic waste as aggregates (0%, 10%, 20% and 30%)	Increase in e-plastic waste reduced the workability and strength of concrete.
Bulut and Sahin, 2017 [6]	E-plastic/filling (0%, 5%, 15% and 25%)	CS increased with the increase in the ratio of resin. The ratio of resin at 15% and e-plastic/filling at 5% were optimum content for CS. Use of 5% e-waste in polymer concrete did not had negative effect in concrete.
Martínez et al., 2019 [13]	Gamma irradiated polycarbonate particles (3%, 6% and 15%) as aggregates	The gamma irradiated polycarbonate particles as aggregates in concrete increased the CS.
Needhidasan et al., 2019 [14]	E-waste plastic as CA (0%, 12%, 17% and 22%)	Addition of e-waste powder increased the workability, CS, STS and FS.
Santhanam et al., 2019 [15]	E-waste plastic as CA (0%-20%)	E-waste plastic decreased the unit weight, CS and FS and increased the slump value and STS.
Shinu and Needhidasan, 2019 [16]	E-waste plastic as CA (12%, 17% and 22%)	Unit weight of consisting e-waste plastic reduced. E-waste plastic reduced the CS, STS and FS of concrete.
Needhidasan et al., 2019 [17]	E-waste plastic as CA (0%, 10% and 12.5%)	E-waste plastic decreased the slump, CS and FS but increased the STS.
Santhanam and Anbuarasu, 2019 [18]	E-waste plastic as CA (0%, 8%, 12% and 16%)	Increase in e-waste plastic content decreased the slump value and increased the CS, STS and FS.
Needhidasan and Sai, 2020 [19]	E-plastic waste as CA (0%, 8%, 12% and 16%) and fly ash	Increase in e-plastic waste decreased the slump value and increased CS, STS and FS.
Evram et al., 2020 [20]	Waste electronic waste as aggregates (0%, 10%, 20%, 30%, 40%); and waste marble dust (MD) as cement substitution (0%, 5%, 10%, 15%)	The addition of MD decreased the slump and improved the strength of concrete. The increase in e-plastic reduced the need of SP, strength, elastic modulus and unit weight.
Mane et al., 2020 [21]	E-waste as partial substitution of manufactured fine aggregates (M-sand) (0%, 10%, 20%, 30% and 40%)	Workability decreased with the increase in e-waste content. The optimum content of e-waste substitution was 20% in terms of strength and chloride permeability.
Bharani et al., 2020 [22]	Steel slag by sand (10%, 20%, 30%) and E-waste by CA (0%, 10%, 20%, 30%)	The steel slag at 20% and 20% steel slag+20% e-waste had optimum replacement content in terms of strength of concrete.
S, 2020 [23]	E-plastic waste as CA (10%, 20%, 30%)	At 10% E-waste slump value increased afterward it decreased. The e-plastic waste upto 20% enhanced the strength afterward it decreased.
Raju et al., 2020 [24]	LCD glass powder as partial substitution to cement (5%, 10%, 15% and 20%)	The waste at 5% had the optimum content in terms of strength, sorptivity and chloride ion penetration. LCD glass powder at 20% had better performance against sulphate and acid attack
Rajkumar et al., 2020 [25]	Electronic waste (EW) (0%, 5%, 10%, 15%, 20%) and jute fibre (JF) (0%, 0.5%, 1%, 2%)	The slump value decreased with EW and JF. JF (1%) and EW (15%) had the optimum content for strength and JF was more effective.
Kalpana et al., 2020 [1]	E-waste as fine aggregate at 10%, 15%, 20% and 25%	Addition of e-waste upto 15% in concrete increased the CS, STS and FS.
Suleman and Needhidasan, 2020 [26]	E-plastic waste as partial substitution to FA (0%, 5.5%, 11%, 16.5%)	Increase in e-plastic waste reduced the workability. The e-plastic waste upto 5.5% increases the CS afterward it decreased. STS and FS increased with e-plastic waste upto 11% afterward it declined.

DOI: https://doi.org/10.30564/jbms.v2i2.2759

The increase in e-plastic reduced the need of SP to maintain the slump value due to zero water absorption capacity and smooth texture of e-plastic. MD decreased the slump too [20]. The slump value decreased with the addition of EW and JF as compared to plain mix [25]. Workability of concrete increased with the increase in e-waste plastic content due to its lower water absorption capacity [14-15].

2.2.2 Hardened Properties

CS increased with the increase in the ratio of resin due to strong adherence because of resin's better wetting and covering the filling materials. The ratio of resin at 15% and e-plastic/filling at 5% were optimum content for CS. Increase in resin ratio increased FS upto 15% then reduced slightly. The optimum resin/filling ratio and e-plastic/filling ratio were 15-85% and 5- 15% for STS. Use of 5% e-waste in polymer concrete did not have negative effect in concrete [6]. The gamma irradiated polycarbonate particles as aggregates in concrete increased CS and the lowest strength was obtained at 3% [13].

The inclusion of MD enhanced the performance of concrete due to filling effect. Strength, elastic modulus and unit weight reduced as compared to reference mix due to smooth surface, lower modulus of elasticity and strength of e-plastic aggregates. The minimum reduction in CS and toughness was at 20% e-waste [20]. The density and strength of concrete decreased with the increase in e-plastic waste due to reduction in adhesive strength between the materials and its hydrophobic nature restrict the cement hydration; high porosity and poor bonding between plastic waste and cement mortar [11, 12, 16]. The optimum content of e-waste substitution was 20% in terms of strength and chloride permeability due to optimal size distribution formation of dense microstructure and low bond strength of plastic waste [21, 23]. The steel slag at 20% and 20% steel slag+20% e-waste had optimum replacement content in terms of strength of concrete [22]. Waste PCB increased the air content and water retention property and decreased the bulk density of mortar. Waste PCB less than 15% did not decrease CS and FS rapidly afterward it decreased gradually [10]. The waste at 5% had the optimum content in terms of strength, sorptivity and chloride ion penetration due to the improved structure. LCD glass powder at 20% had better performance against sulphate and acid attack [24]. JF (1%) and EW (15%) had the optimum replacement content for strength. JF gave high strength and stability as it reduces the crack formation [25]. Addition of e-waste upto 15% in concrete increased the CS, STS and FS [1]. Increase in e-plastic waste increased CS, STS and FS [14, 18, 19]. E-waste plastic decreased the unit weight, CS and FS and increased the STS [15]. E-plastic waste upto 5.5% increases the CS afterward it decreased. STS and FS increased with e-plastic waste upto 11% afterward it declined [26]. E-waste plastic decreased the CS and FS but increased the STS [17].

3. Conclusions

In today world, people are very much dependant on the electric and electronic devices for routine daily life activity. With very fast advancement in technology, older devices are replaced with new and better one. The former becomes the waste and thus generation of electronic wastes is becoming the serious threat to the environment and human health. The reuse of electronic waste in the construction industry may conserve the natural resources and reduce the waste problems. A review has studied on the utilization of wastes into concrete and bitumen. Increase in e-waste in bitumen increased the penetration value, softening point, viscosity, specific gravity and decreased the ductility value. The addition of electronic waste decreased the slump value of concrete. Up to the certain limit, e-waste as aggregates in concrete improved the strength and durability characteristics. Therefore, the electronic waste can be effectively used as construction materials. The utilization of wastes in the concrete promotes the reuse of these wastes and solves the disposal problem.

References

[1] Kalpana M, Vijayan DS, Benin SR. Performance study about ductility behaviour in electronic waste concrete. Materials Today: Proceedings 2020. https://doi.org/10.1016/j.matpr.2020.07.049 .

[2] Needhidasan S, Agarwal SG. A review on properties evaluation of bituminous addition with E-waste plastic powder. Materials Today: Proceedings 2019. https://doi.org/10.1016/j.matpr.2019.12.127.

[3] Santhanam N, Anbuarasu G. Experimental study on high strength concrete (M60) with reused E-waste plastics. Materials Today: Proceedings 2019. https://doi.org/10.1016/j.matpr.2019.11.107.

[4] Kumar A, Devi K, Singh M, Soni DK. Significance of stone waste in strength improvement of soil. Journal of Building Material Science 2019;1:32-36.

[5] Devi K, Saini B, Aggarwal P. Utilization of Kota stone slurry powder and accelerators in concrete. Computers and Concrete 2019;23:189-201.

[6] Bulut HA, Sahin R. A study on mechanical properties of polymer concrete containing electronic plastic waste. Composite Structures 2017;178:50-62.

[7] Zhang L, Xu Z. Towards minimization of secondary wastes: Element recycling to achieve future com-

 DOI: https://doi.org/10.30564/jbms.v2i2.2759

plete resource recycling of electronic wastes. Waste 2019;96:175-180.

[8] Santhanam N, Ramesh B, Agarwal SG. Experimental investigation of bituminous pavement (VG30) using E-waste plastics for better strength and sustainable environment. Materials Today: Proceedings 2019. https://doi.org/10.1016/j.matpr.2019.12.057.

[9] Kumar GR, Santhosh KS, Bharani S. Influence of E-waste on properties of bituminous mixes. Materials Today: Proceedings 2020. https://doi.org/10.1016/j.matpr.2020.08.539.

[10] Wang R, Zhang T, Wang P. Waste printed circuit boards nonmetallic powder as admixture in cement mortar. Materials and Structures 2012;45:1439-1445.

[11] Kumar KS, Baskar K. Recycling of E-plastic waste as a construction material in developing countries. J Mater Cycles Waste Manag 2015;17:718-724.

[12] BT AM. 2016. Partial replacement of E-plastic Waste as Coarse-aggregate in Concrete. Procedia Environmental Sciences 2016;35:731-739.

[13] Martínez AL De la C, Barrera GM, Díaz CEB, Córdoba LIÁ, Núñez FU, Hernández DJD. Recycled polycarbonate from electronic waste and its use in concrete: Effect of irradiation. Construction and Building Materials 2019;201:778-785.

[14] Needhidasan S, Vigneshwar CR, Ramesh B. Amalgamation of E-waste plastics in concrete with super plasticizer for better strength. Materials Today: Proceedings 2019. https://doi.org/10.1016/j.matpr.2019.11.253.

[15] Santhanam N, Ramesh B, Pohsnem FK. Concrete blend with E-waste plastic for sustainable future. Materials Today: Proceedings 2019. https://doi.org/10.1016/j.matpr.2019.11.204.

[16] Shinu NMMT, Needhidasan S. An experimental study of replacing conventional coarse aggregate with E-waste plastic for M40 grade concrete using river sand. Materials Today: Proceedings 2019. https://doi.org/10.1016/j.matpr.2019.09.033.

[17] Needhidasan S, Ramesh B, Prabu SJR. Experimental study on use of E-waste plastics as coarse aggregate in concrete with manufactured sand. Materials Today: Proceedings 2019. https://doi.org/10.1016/j.matpr.2019.10.006.

[18] Santhanam N, Anbuarasu G. Experimental study on high strength concrete (M60) with reused E-waste plastics. Materials Today: Proceedings 2019. https://doi.org/10.1016/j.matpr.2019.11.107.

[19] Needhidasan S, Sai P. Demonstration on the limited substitution of coarse aggregate with the E-waste plastics in high strength concrete. Materials Today: Proceedings 2020; 22:1004-1009.

[20] Evram A, Akçaogˇlu T, Ramyar K, Çubukçuogˇlu B. Effects of waste electronic plastic and marble dust on hardened properties of high strength concrete. Construction and Building Materials 2020;263;120928.

[21] Mane KM, Nadgouda PA, Joshi AM. An experimental study on properties of concrete produced with M-sand and E- sand 2020. https://doi.org/10.1016/j.matpr.2020.08.086.

[22] Bharani S, Rameshkumar G, Manikandan J, Balayogi T, Gokul M, Bhuvanesh DC. Experimental investigation on partial replacement of steel slag and E-waste as fine and coarse aggregate. Materials Today: Proceedings 2020. https://doi.org/10.1016/j.matpr.2020.09.419.

[23] S Arivalagan. Experimental Study on the Properties of Green Concrete by Replacement of E-Plastic Waste as Aggregate. Procedia Computer Science 2020;172:985-990.

[24] Raju AS, Anand KB, Rakesh P. Partial replacement of Ordinary Portland cement by LCD glass powder in concrete. Materials Today: Proceedings 2020. https://doi.org/10.1016/j.matpr.2020.10.661.

[25] Rajkumar R, Ganesh VN, Mahesh SR, Vishnuvardhan K. Performance evaluation of E-waste and Jute Fibre reinforced concrete through partial replacement of Coarse Aggregates. Materials Today: Proceedings 2020. https://doi.org/10.1016/j.matpr.2020.10.689.

[26] Suleman S, Needhidasan S. Utilization of manufactured sand as fine aggregates in electronic plastic waste concrete of M30 mix. Materials Today: Proceedings 2020. https://doi.org/10.1016/j.matpr.2020.08.043.

DOI: https://doi.org/10.30564/jbms.v2i2.2759

BILINGUAL PUBLISHING CO.
Pioneer of Global Academics Since 1984

Journal of Building Material Science
https://ojs.bilpublishing.com/index.php/jbms

ARTICLE

Modeling and Simulation of Wood and Fly Ash Behaviour as Partial Replacement for Cement on Flexural Strength of Self Compacting Concrete

Eluozo S.N.[2*] **Dimkpa K.**[1]

1.Department of Architecture, Faculty of Environmental Science, Rivers State University, Nkpolu Oroworukwo, Port Harcourt, Nigeria
2.Department of Civil Engineering, College of Engineering, Gregory University Uturu (GUU), Abia State, Nigeria

ARTICLE INFO

Article history
Received:8 March 2021
Accepted:25 April 2021
Published Online:15 May 2021

Keywords:
Modeling
Wood fly ash partial cement
Flexural strength

ABSTRACT

Flexural strength was monitored and predicted on the application improving concrete strength with wood and fly as partial replacement for cement. The study observed the pressure from the constituent of these locally sourced material that has been observed from the study to influence the flexural strength through the effect from this locally sourced addictives. The study monitors concrete porosity on heterogeneity as it reflect on the flexural strength of self compacting concrete. Other condition considered was the compaction and placement of concrete. These effects were monitored at constant water cement ratio from design mix. The behaviour from this effects on the concrete observed the rate of flexural growth under the influences of these stated conditions. The simulation expressed the reactions of these effects through these parameters monitored to influence the system. Numerical simulations were also applied to the optimum curing age of twenty eight days, while analytical simulation was also applied. This concept is the conventional seven days interval that concrete curing were observed, these are improvement done on the study carried out by experts [16]. These locally sourced material were experimentally applied. The simulation predictive values are at the interval of seven days of curing, which was also simulated. The predictive values were compared with the experimental values of the researchers [16], and both values developed best fits correlations. The study is imperative because the system considered the parameters used on experimental and observed other influential variables that were not examined. These were not observed in the experimental procedure. Experts in concrete engineering will definitely find these concept a better option in monitoring flexural strength of self compacting concrete in general.

1. Introduction

There has been the exhibition of mechanical properties on High-Strength Concrete (HSC), two groups on these properties can be separated as short terms, known to be mechanical properties, and long-term mechanical properties. The stress strain from concrete on HSC are fundamentals that determine design model, it also includes the

**Corresponding Author:*
Eluozo S.N.,
Department of Civil Engineering, College of Engineering, Gregory University Uturu (GUU), Abia State, Nigeria;
Email: ndusolo2018@gmail.com

 DOI: https://doi.org/10.30564/jbms.v2i2.2948

behaviour of the materials parameters, aggregates type are included through experimental values such as curing age at testing, the strain rate includes other level of interaction between the specimen and testing machine. The stress-strain model that is applied for NSC cannot be lengthy when it applied for HSC; it is observed from basis of loading curve that will definitely change it significantly [12,13,14,15]. Researchers through studies carried out have express the rising of steeper that observed sudden drop in strength after attaining a maximum value; this concept was developed from present numerical modeling on concrete stress-strain behaviour of HSC. [1,2,3] The study has recommended that HSC performs like a real composite material; it's also equivalents of stress-strain that can be drawn to the applied developed concept in rock mechanic [5,6,7]. [9] observed that it is observed to experienced less internal microcracking in HSC. This implies that it is more than that of NSC for the same axial strain imposed. It has been observed that HSC experience a smaller amount lateral strain, and consequently it has a level of efficiency internment on compressive strength. HSC is limited compared to that of NSC. Water cement ratios reduction [w/c] experienced increases the strength of concrete using locally 3/8 all-one aggregate [10]. Nevertheless, hydrated cement strength is low if it is associated with the strength of coarse aggregates. The Comparison carried out between it very important that strength and quality of coarse aggregates should increase, more so together with other factors. Typically, w/c ratios between 0.2- 0.4 are applied for HSC. Meanwhile it is observed that Low w/c ratio decreases its workability. [12,14,15,16] evaluates the influence of silica fume on strength development of HSC coring age between 7 to 28 days after mixing. Compressive strength measured on HSC is determined based on testing variables, which includes mold type, specimen size, end conditions and strain rate. 4×8 in. (102×204 mm), it also involves cylinder specimens that have been shown to generate (ACI, 2010). ACI-318 (ACI, 2011), it also defines the secant modulus of elasticity based on the ratio of stress and strain at 40% of the compressive strength. As strength of concrete experience increases, its modulus of elasticity also observed an increases, while Poisson's ratio is not affected by compressive strength, this could be through curing method age of concrete [5,6,8,10,12].

2. Theoretical Background

$$\frac{d_{c_d}}{dx} + V(y)c_d = (y)c_d^n \tag{1.0}$$

Dividing equation (1.0) all through by c_d^n. we have

$$c_d^{-n}\frac{d_{c_d}}{dx} + v(x)c_d^{1-n} = (y) \tag{1.1}$$

Let

$$P = c_d^{1-n}. \tag{1.2}$$

$$\frac{dp}{dy} = (1-n)c_d^{-n}\frac{d_{c_d}}{dy}$$

$$c_d^{-n}\frac{d_{c_d}}{dy} = \frac{1}{1-n}\frac{dp}{dy}. \tag{1.3}$$

Substituting equation (1.2) and (1.3) into equation (1.1) we have that

$$\frac{1}{1-n}\frac{dp}{dx} + V(y)p = (y). \tag{1.4}$$

tegrating both sides we have

$$\int d\left[e^{V(y)(1-n)y}p\right] = (y)(1-n)\int e^{V(y)(1-n)y}dy.$$

$$p = \frac{(y)}{Vu(y)} + Ae^{-Vu(y)(1-n)y}. \tag{1.5}$$

tituting equation (1.2) into equation (1.13) we have

$$c_d^{1-n} = \frac{(y)}{Vu(y)} + Ae^{-Vu(y)(1-n)y} \tag{1.6}$$

3. Materials and Method

3.1 Flexural and Tensile Strength

Concrete has relatively high compressive strength in the range of 10 to 50 Nmm^2 and 60 to 120 Nmm^2 for high strength concrete. Tensile strength significantly low constitutes about 10% of the compressive strength (Neville & Brooks, 1996; Popovics, 1998).

Flexural test is done to find out the tensile strength of concrete. A typical set up recommended by British Standard is illustrated in Figure 1.

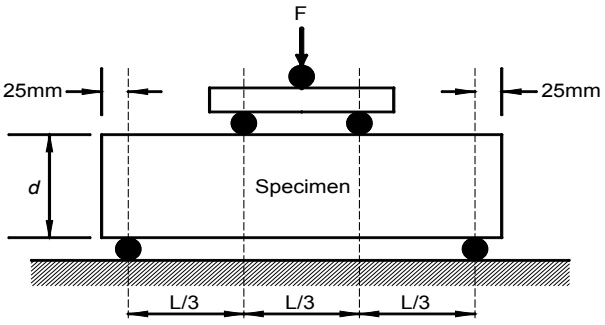

Figure 1. Flexural Beam Test Set-ups

DOI: https://doi.org/10.30564/jbms.v2i2.2948

From mechanics of materials and analysis of Figure 1, maximum tensile stress is expected to occur at the bottom of the constant moment region within which pure bending occurs. The modulus of rapture can be calculated as:

$$f_{tb} = \frac{FL}{bd^2} \quad 3.1$$

Where L= Span of specimen beam
F= maximum applied loads
b= breadth of beam
d= depth of beam

Other method used in determining the tensile strength of concrete is the indirect tension test (split cylinder test or Brazilian test) BS 1881: Part 117:1983 and ASTM C496-71. As recommended in these standards, the splitting test is done by applying compression loads at a loading rate 0.0112 to 0.0231 MPa/s along two axial lines that are diametrically opposite on a specimen 150 x 300 mm cylinder.

4. Results and Discussion

Predictive from Derive model Simulation and Experimental Values of Flexure Strength are in Graphical Presentation and Tables.

Table 1. Predictive and Experimental Values of Flexural Strength at Different Curing Age

Curing Age	Predictive Values of Flexural Strength	Experimental Values of Flexural Strength
7	7.290147108	7.203
8	7.304122385	7.226
9	7.318276351	7.249
10	7.33261129	7.272
11	7.347129516	7.295
12	7.361833373	7.318
13	7.376725235	7.341
14	7.391807504	7.364
15	7.407082616	7.387
16	7.422553037	7.41
17	7.438221263	7.433
18	7.454089823	7.456
19	7.47016128	7.479
20	7.486438228	7.502
21	7.502923293	7.525
22	7.519619138	7.548
23	7.536528456	7.571
24	7.553653977	7.594
25	7.570998467	7.617
26	7.588564724	7.64
27	7.606355584	7.663
28	7.624373919	7.686

Table 2. Predictive and Experimental Values of Flexural Strength at Different Curing Age

Curing Age	Predictive Values of Flexural Strength[W/C-0.35]	Experimental Values of Flexural Strength [W/C-0.35
7	7.009346574	6.999
8	7.02154282	7.012
9	7.033876586	7.025
10	7.046349423	7.038
11	7.058962898	7.051
12	7.071718598	7.064
13	7.084618126	7.077
14	7.097663104	7.09
15	7.110855171	7.103
16	7.124195987	7.116
17	7.137687229	7.129
18	7.151330593	7.142
19	7.165127793	7.155
20	7.179080565	7.168
21	7.193190663	7.181
22	7.207459861	7.194
23	7.221889953	7.207
24	7.236482752	7.22
25	7.251240094	7.233
26	7.266163834	7.246
27	7.281255848	7.259
28	7.296518033	7.272

Table 3. Predictive and Experimental Values of Flexural Strength at Different Curing Age

Curing Age	Predictive Values of Flexural Strength	Experimental Values of Flexural Strength
7	7.025133782	7.525
14	7.992358786	7.952
21	8.091346222	8.281
28	8.392420249	8.432

Table 4. Predictive and Experimental Values of Flexural Strength at Different Curing Age

Curing Age	Predictive Values of Flexural Strength [W/C-0.35]	Experimental Values of Flexural Strength [W/C-0.35]
7	7.199053635	7.029
14	7.506583612	7.505
21	7.829833947	7.981
28	8.36704706	8.454

 DOI: https://doi.org/10.30564/jbms.v2i2.2948

Table 5. Predictive and Experimental Values of Flexural Strength at Different Curing Age

Curing Age	Predictive Values of Flexural Strength	Experimental Values of Flexural Strength
7	7.878527419	7.87441
8	7.891488403	7.88676
9	7.904603993	7.89929
10	7.917876033	7.912
11	7.93130639	7.92489
12	7.944896953	7.93796
13	7.958649631	7.95121
14	7.97256636	7.96464
15	7.986649095	7.97825
16	8.000899817	7.99204
17	8.015320531	8.00601
18	8.029913263	8.02016
19	8.044680066	8.03449
20	8.059623015	8.049
21	8.074744214	8.06369
22	8.090045786	8.07856
23	8.105529885	8.09361
24	8.121198687	8.10884
25	8.137054395	8.12425
26	8.15309924	8.13984
27	8.169335477	8.15561
28	8.18576539	8.17156

Table 6. Predictive and Experimental Values of Flexural Strength at Different Curing Age

Curing Age	Predictive Values of Flexural Strength [W/C-0.35]	Experimental Values of Flexural Strength [W/C-0.35
7	7.86456235	7.85794
8	7.875352825	7.86784
9	7.886251855	7.87786
10	7.897260532	7.888
11	7.908379959	7.89826
12	7.91961125	7.90864
13	7.930955532	7.91914
14	7.942413939	7.92976
15	7.953987622	7.9405
16	7.965677739	7.95136
17	7.977485461	7.96234
18	7.989411973	7.97344
19	8.001458468	7.98466
20	8.013626154	7.996
21	8.02591625	8.00746
22	8.038329989	8.01904
23	8.050868612	8.03074
24	8.063533378	8.04256
25	8.076325554	8.0545
26	8.089246423	8.06656
27	8.10229728	8.07874
28	8.115479431	8.09104

Table 7. Predictive and Experimental Values of Flexural Strength at Different Curing Age

Curing Age	Predictive Values of Flexural Strength	Experimental Values of Flexural Strength
7	7.075858436	7.044
14	7.424520654	7.382
21	8.176343921	8.068
28	8.393106863	8.334

Table 8. Predictive and Experimental Values of Flexural Strength at Different Curing Age

Curing Age	Predictive Values of Flexural Strength [W/C-0.35]	Experimental Values of Flexural Strength [W/C-0.35]
7	6.833394616	7.65794
14	7.391165982	7.72976
21	8.337609706	8.00746
28	8.217817623	8.19704

Table 9. Predictive and Experimental Values of Flexural Strength at Different Curing Age

Curing Age	Predictive Values of Flexural Strength	Experimental Values of Flexural Strength
7	6.888260628	6.881
8	6.904492123	6.895
9	6.920961562	6.909
10	6.937672434	6.923
11	6.954628276	6.937
12	6.971832682	6.951
13	6.989289294	6.965
14	7.007001809	6.979
15	7.02497398	6.993
16	7.043209612	7.007
17	7.061712568	7.021
18	7.080486766	7.035
19	7.099536182	7.049
20	7.118864852	7.063
21	7.138476869	7.077
22	7.158376387	7.091
23	7.178567619	7.105
24	7.199054843	7.119
25	7.219842398	7.133
26	7.240934686	7.147
27	7.262336175	7.161
28	7.284051397	7.175

DOI: https://doi.org/10.30564/jbms.v2i2.2948

Table 10. Predictive and Experimental Values of Flexural Strength at Different Curing Age

Curing Age	Predictive Values of Flexural Strength [W/C-0.35]	Experimental Values of Flexural Strength [W/C-0.35]
7	6.870820879	6.866
8	6.884291658	6.878
9	6.897928946	6.89
10	6.911734801	6.902
11	6.925711307	6.914
12	6.939860574	6.926
13	6.954184736	6.938
14	6.968685956	6.95
15	6.983366423	6.962
16	6.998228351	6.974
17	7.013273984	6.986
18	7.028505593	6.998
19	7.043925476	7.01
20	7.059535961	7.022
21	7.075339404	7.034
22	7.091338189	7.046
23	7.107534731	7.058
24	7.123931476	7.07
25	7.140530896	7.082
26	7.157335499	7.094
27	7.174347819	7.106
28	7.191570424	7.118

Table 11. Predictive and Experimental Values of Flexural Strength at Different Curing Age

Curing Age	Predictive Values of Flexural Strength	Experimental Values of Flexural Strength
7	6.239583526	6.237
14	6.613762412	6.447
21	7.815783049	7.574
28	8.341567593	8.366

Table 12. Predictive and Experimental Values of Flexural Strength at Different Curing Age

Curing Age	Predictive Values of Flexural Strength [W/C-0.35]	Experimental Values of Flexural Strength [W/C-0.35]
7	6.219641662	6.223
14	6.568781151	6.318
21	7.761391953	7.449
28	8.328009693	8.315

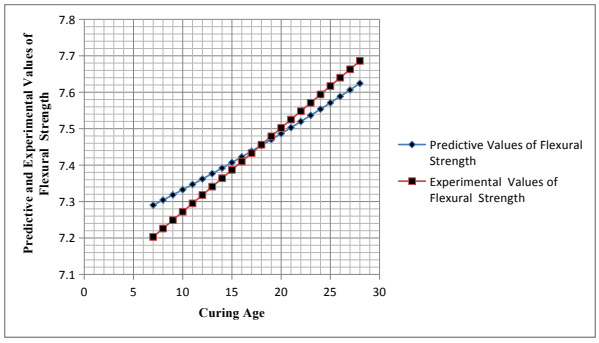

Figure 2. Predictive and Experimental Values of Flexural Strength at Different Curing Age

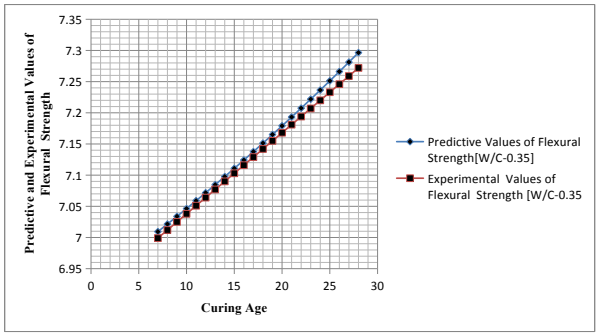

Figure 3. Predictive and Experimental Values of Flexural Strength at Different Curing Age

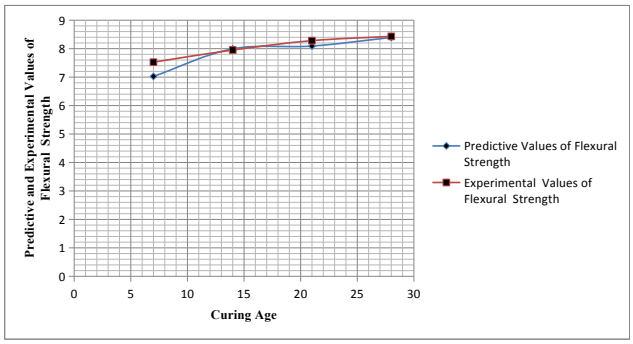

Figure 4. Predictive and Experimental Values of Flexural Strength at Different Curing Age

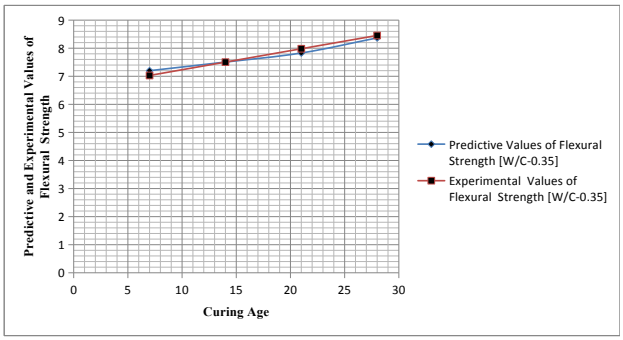

Figure 5. Predictive and Experimental Values of Flexural Strength at Different Curing Age

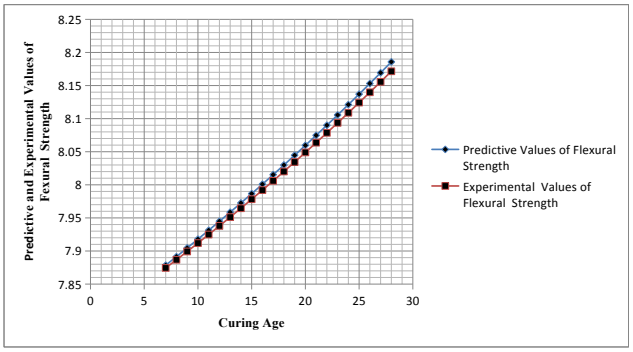

Figure 6. Predictive and Experimental Values of Flexural Strength at Different Curing Age

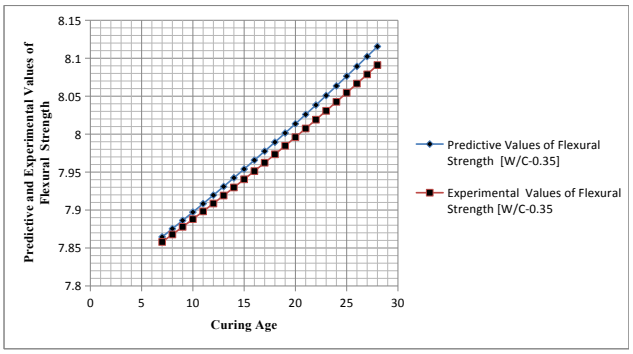

Figure 7. Predictive and Experimental Values of Flexural Strength at Different Curing Age

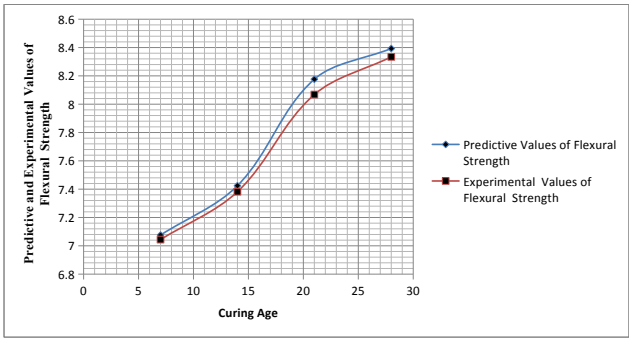

Figure 8. Predictive and Experimental Values of Flexural Strength at Different Curing Age

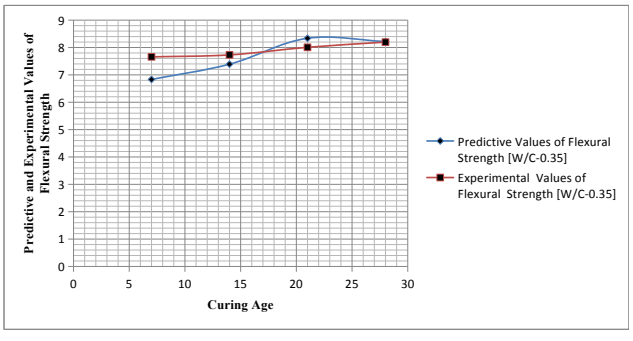

Figure 9. Predictive and Experimental Values of Flexural Strength at Different Curing Age

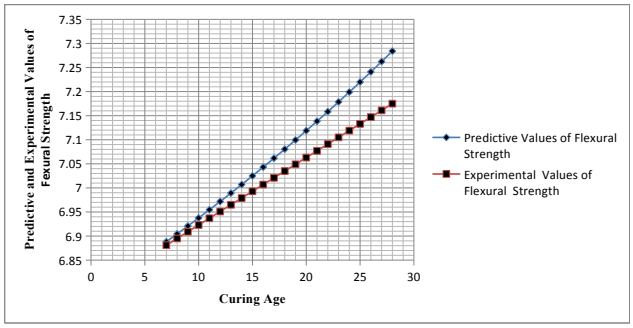

Figure 10. Predictive and Experimental Values of Flexural Strength at Different Curing Age

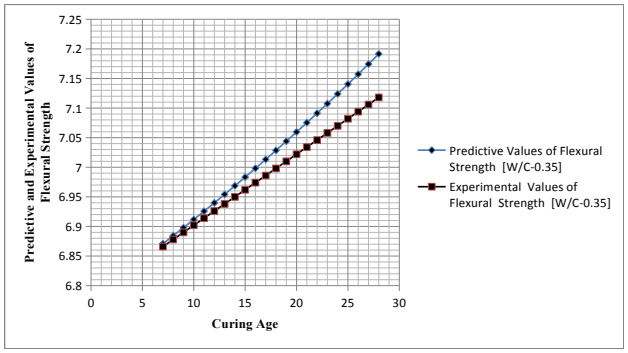

Figure 11. Predictive and Experimental Values of Flexural Strength at Different Curing Age

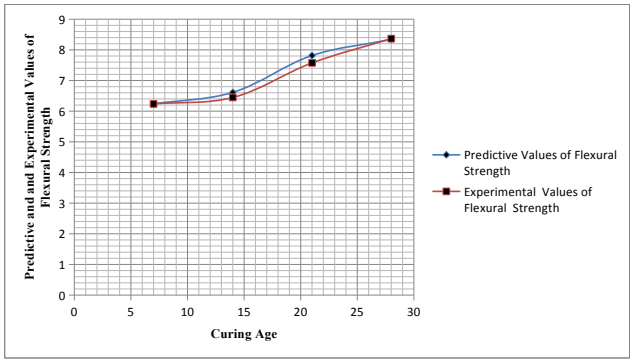

Figure 12. Predictive and Experimental Values of Flexural Strength at Different Curing Age

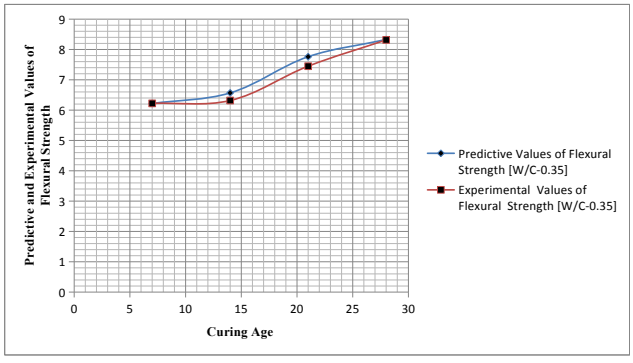

Figure 13. Predictive and Experimental Values of Flexural Strength at Different Curing Age

DOI: https://doi.org/10.30564/jbms.v2i2.2948

Figure 2-13 explained the heterogeneous behaviour of flexural strength from concrete partially replace cement with wood and fly ash. The study observed linear growth rate from the numerical applied in some parts of the simulation, why some part of the figures expressed gradual increase, and at a certain level sight increase on the growth rate were experienced. These were in accordance with the conventional growth rate of concrete. The study monitored the effects from other parameters that were observed to reflect its reaction on the heterogeneous growth rate of the flexural strength. These parameters considered in the system simulation are porosities and compaction of concrete that generates the flexural strength. The study observed the variation rate of influence on the growth rate of the flexural strength based on these factors. Constant water cement ratios were applied on the simulation, and this were also monitored to see its heterogeneous reflection on flexural strength. The derived model were simulated, examined and observed the heterogeneous behaviour of flexural as it also reflects on its mechanical properties. The predictive were compare with the experimental values of SachinPrabhu et al 2018, and both parameters developed best fits correlation.

5. Conclusions

Flexural strength was developed from a mixed design that partially replaced cement with wood and fly ash on self compacting concrete. The study applied these locally sourced materials that developed a mixed design to generates flexural strength. The behaviour of the material on the target concrete strength generated the flexural strength under the influenced of the locally sourced addictives. The system was monitored considering the dosage of the addictive at different percentage in the mixed design. The self compacting concrete with partial replacement cement with wood and fly ash was thoroughly examined through these simulation. The reactions of these self compacting concrete were expressed experimentally by SachinPrabhu et al 2018. The predictive and the experimental values expressed best fits correlation. The study has expressed the effect from other parameters that improve the study done by SachinPrabhu et al 2018. Other improvement was carried out applying numerical simulation to monitor the growth rate of the flexural strength at every twenty four hour. The increase in flexural strength increase in the study were thoroughly evaluated.

References

[1] ACI (2010). "Report on high strength concrete." Report ACI 363R-10, Farmington Hills, MI, American Concrete Institute.

[2] ACI (2011). "Building code requirements for structural concrete and commentary." Report ACI 318-11, American Concrete Institute, USA.

[3] Ahmad, S., and Shah, S. (1982). "Stress-strain curves of concrete confined by spiral reinforcement." ACI.

[4] Carrasquillo, R. L., Nilson, A. H., and Slate, F. O. (1981). "Properties of high-strength concrete subject to short-term loads." Journal of the American Concrete Institute, 78(3), 171-178.

[5] Iravani, S. (1996). "Mechanical properties of high-performance concrete." ACI Materials Journal, 93(5), 416-426.

[6] Logan, A., Choi, W., Mirmiran, A., Rizkalla, S., and Zia, P. (2009). "Short-term mechanical properties of high-strength concrete." ACI Materials Journal, 106(5), 413.

[7] Shah, S., and Ahmad, S. (1994). "High performance concrete: properties and applications." New York, McGraw-Hill.

[8] Zhaoyu M; Moses M Mechanical Properties of High-Strength Concrete PhD Candidate, Department of Civil, Structural and Environmental Engineering, University at Buffalo, State University of New York.

[9] Perenchio, W. F., and Klieger, P. (1978). "Some physical properties of high-strength concrete." Portland Cement Association.

[10] Whittaker, A. S. (2012). "CIE 525: Concrete Design Class Notes."University at Buffalo, NY.

[11] Wight, J. K., and MacGregor, J. G. (2009). "Reinforced concrete: Mechanics and design (5th edition)." Pearson Prentice Hall, Upper Saddle River, NJ.

[12] Ephraim M.E. Ode .T. (2006) Specification for structural Application of concrete with 10mm (3/8) All – in Gravel Aggregate NEAM Vol 1 No 1.

[13] Eluozo, S.N. Ode .T. (2015) Mathematical model to monitor stiff clay compression index in wet land area of Degema Volume 6, Issue 12, pp. 59-72, Article ID: IJARET_06_12_007.

[14] Eluozo, S.N. Ode .T. (2015) Mathematical model to predict compression index of uniform loose sand in coastal area of Degema, Rivers State of Nigeria. International Journal of Advanced Research in Engineering and Technology Volume 6, Issue 12, pp. 86-103, Article ID: IJARET_06_12_009.

[15] Eluozo. S. N and Ode T, Modeling and Simulation of Compression Strength for Firm Clay in Swampy Area of Ahoada East. International Journal of Advanced Research in Engineering and Technology, 6(12), 2015, pp. 73-85.

 DOI: https://doi.org/10.30564/jbms.v2i2.2948

BILINGUAL
PUBLISHING CO.
Pioneer of Global Academics Since 1984

Tel:+65 65881289
E-mail:contact@bilpublishing.com
Website:www.bilpublishing.com

ISSN 2630-5216
02
9 772630 521200